THE UNIVERSITY OF

COLLEGE OF ENGIN]
Department of Aeronautical and Ast
Aircraft Propulsion L

THE EFFECT OF THE BOUNDARY LAYER UPON THE FLOW IN A CONICAL HYPERSONIC WIND TUNNEL NOZZLE

by

Martin Sichel

ORA Project 02953

under contract with:

Department of the Navy
Office of Naval Research
Mathematical Sciences Division
Washington, D. C.
Contract No. Nonr-1224(31) NR 061-108

administered through:

OFFICE OF RESEARCH ADMINISTRATION ANN ARBOR

July 1963

TABLE OF CONTENTS

	Page
LIST OF FIGURES	iv
SUMMARY	v
ACKNOWLEDGMENT	v
NOMENCLATURE	vi
I. INTRODUCTION	1
II. FLOW IN THE HYPERSONIC NOZZLE	3
A. Formulation of Integral Equations for Nozzle Flow	3
B. Discussion of the Nozzle Integral Equations	8
C. Approximate Hypersonic Solutions of the Nozzle Momentum Integral Equations	17
III. CALCULATION OF HYPERSONIC NOZZLE FLOW USING EMPIRICAL RELATIONS FOR THE BOUNDARY LAYER DISPLACEMENT THICKNESS	29
IV. DISCUSSION AND CONCLUSIONS	37
REFERENCES	42
APPENDIX A	
APPENDIX B	
APPENDIX C	

LIST OF FIGURES

Figure

1. Conical Nozzle Boundary Layer Coordinate System.
2. Approximate Nozzle Velocity Distribution for the Case $\theta_w << 1$.
3. Arc Chamber Conditions for Equilibrium Air.
4. Variation of Test Section Boundary Layer Thickness with Stagnation Conditions.
5. The Mach Number Function ϕ for Equilibrium Air.
6. Variation of Test Section Mach Number with Stagnation Conditions.
7. The Effect of the Boundary Layer upon the Test Section Mach Number.
8. Variation of Test Section Static Pressure with Stagnation Conditions.
9. The Effect of the Boundary Layer upon the Test Section Static Pressure.
10. Variation of Test Section Static Temperature with Stagnation Conditions.
11. Variation of Test Section Density and Limiting Velocity with Stagnation Conditions.
12. The Effect of the Boundary Layer upon the Test Section Density.

A-1. Mass Flow Correction Factor E $\sigma; \frac{\delta^*}{R}$

C-1. Area Ratio Correction Factor $f_1 (h_o, p_o)$.

C-2. Mass Flow Correction Factor $f_2 (h_o, p_o)$.

C-3. Ratio of Average to Ideal Gas Specific Heat, $f_3 (p, h^*)$.

C-4. Variation of the Boundary Layer Thickness with the Function ζ.

SUMMARY

Integral equations for the flow in a conical hypersonic nozzle with a thick boundary layer have been formulated and some approximate solutions of these equations have been studied. A method developed by Burke[3] for calculating boundary layer thickness using empirical correlations has been extended to a relatively broad range of stagnation conditions and has been used to compute the effect of boundary layer development upon hypersonic nozzle flow.

ACKNOWLEDGMENT

The work reported here was sponsored by the Office of Naval Research under contract Nonr-1224(31) NR 061-108 for the "Study of High Velocity Flow with Dissociation and Ionization."

The author would like to thank Professor P. M. Sherman for her help and encouragement, and Mr. Stanley Wu who carried out the bulk of the often tedious calculations.

NOMENCLATURE

A_t	throat area
A_{geom}	geometric area
A_{eff}	effective area
α	atom mass fraction
C_P	specific heat at constant pressure
c_f	skin friction coefficient
δ	boundary layer thickness
δ^*	displacement thickness
δ_2	momentum thickness
δ_3	energy thickness
$\overline{\delta^*}$	$\delta^* - \delta^{*2}/2R$
$\overline{\delta_2}$	$\delta_2 - \delta_2^2/2R$
$\overline{\delta_3}$	$\delta_3 - \delta_3^2/2R$
Δ	thermal boundary layer thickness
e_o	stagnation internal energy per unit mass
e_i	initial internal energy per unit mass
H	δ^*/δ_2
$\overline{H}$	$\overline{\delta^*}/\overline{\delta_2}$
H_i	incompressible value of δ^*/δ_2
θ_{uc}	useful core angle
θ_w	nozzle wall angle
h_{aw}	adiabatic recovery enthalpy
h_o	stagnation enthalpy
h	enthalpy
h_A^o	atom heat of formation per unit mass
Le	Lewis number
M	Mach number
$\dot{m}$	mass flow

μ	viscosity
ν	kinematic viscosity
p	pressure
Pr	Prandtl number
q	heat flux
Q_c	arc chamber volume
R	nozzle radius
Re	Reynolds' number
r	radius
r_t	throat radius
ρ	density
St	Stanton number
T	temperature
T_o	stagnation temperature
τ	shear stress
u	velocity
u_e	free stream velocity
V	radial velocity in conical flow
x	distance from nozzle throat
y	distance from wall
ω	viscosity index
γ	ratio of specific heats

Subscripts and Superscripts

aw	adiabatic recovery
e	free stream or core
R	reference value
uc	useful core
w	wall
( )*	quantities evaluated at the Eckert reference temperature

I. INTRODUCTION

In supersonic wind tunnels the boundary layers on the walls of the test section are quite thin and so have only a small effect upon the test section flow. On the other hand in hypersonic tunnels for $M > 4$ the boundary layer occupies an appreciable portion of the test section,[1,2,3] and then the performance of a wind tunnel depends strongly upon the boundary layer behavior. In the present work the effect of the boundary layer upon the test section conditions in a hypersonic wind tunnel with a nozzle of fixed geometry is investigated.

In supersonic wind tunnels with fixed test section to throat area ratio the test section Mach number is constant and the pressure and temperature are directly proportional to the stagnation chamber pressure and temperature. The effect of the boundary layer on the test section flow is essentially of second order[1] and is taken into account by adding the boundary layer displacement thickness to the perfect fluid nozzle contour. Even if this thickness is off by a factor of 2 the effect upon the nozzle flow will be extremely small.

In hypersonic tunnels on the other hand the test section Mach number varies appreciably with stagnation conditions even when the nozzle geometry is fixed, and of course the relation between test section temperature and pressure and stagnation conditions is considerably more complex than in the supersonic case. This drastic change in behavior comes about because, at the high stagnation enthalpies needed to produce hypersonic flow, variations in the molecular weight and specific heat of the test gas during the expansion appreciably affect the flow, and because at these high Mach numbers and temperatures the boundary layer may occupy 50% or more of the test section area. Both of these effects are quite sensitive to the stagnation pressure and enthalpy.

In the design of hypersonic nozzles[4] the contour of the inviscid core of the nozzle can be calculated using the method of characteristics. The boundary layer displacement thickness is then added to the core in order to determine the

hypersonic nozzle contour. The situation is quite different if the variation of test section conditions with stagnation conditions is to be determined for a fixed geometry nozzle. Then because of the preponderance of the boundary layer, and because of the interaction between the boundary layer and the core, the inviscid and boundary layer flows must be computed simultaneously. Thus just as in the case of external hypersonic flows[5] there is a strong interaction between the viscous boundary layer and the external inviscid flow.

The computation of hypersonic nozzle flow thus poses many difficulties. The simple analytic formulae which apply to supersonic isentropic nozzle flows are no longer applicable, and to compute the flow in the inviscid core it becomes necessary to use either gas tables[6-19] or charts[20-27] or to employ empirical formulae[28-35] for the properties of the gas in question. Further there is the question of whether or not the gases in the core are in chemical equilibrium or whether the flow is frozen.[36-45] Usually there is equilibrium until some point beyond the nozzle throat where then over a fairly short region freezing occurs.

Finally in computing nozzle flow it is necessary to determine the thickness of the boundary layer. The stagnation densities under consideration in the present report are sufficiently high that, at least from the discussion of Enkenhus,[4] it appears reasonable to assume that the boundary layer will be turbulent throughout. A laminar boundary layer comes under consideration only in the case of low density tunnels. Boundary layer thicknesses have been calculated by either integrating the VonKarman boundary layer integral equations starting at the throat and contrinuing to the test section[4, 46-51] or by using empirical formulas to compute the boundary layer thickness at the test section directly.[1, 3, 52, 53] Because of a lack of a detailed understanding of turbulence either method of determining the boundary layer thickness is inherently empirical.

In the work below the integral equations for the combined core and turbulent boundary layer flow in a conical hypersonic nozzle are derived. Assumptions and empirical relations required to solve these integral equations are discussed;

however, an exact solution of these equations is beyond the scope of the present study. Finally, empirical boundary layer thickness correlations have been used to compute the effect of boundary layer development upon the performance of a specific nozzle over a wide range of stagnation conditions.

II. FLOW IN THE HYPERSONIC NOZZLE

A. Formulation of Integral Equations for Nozzle Flow

The problem at hand is the simultaneous solution of the conservation equations in both the inviscid core and the boundary layer of the tunnel nozzle. Schlichting[54] and Atkinson and Goldstein[55] have calculated the simultaneous development of the incompressible boundary layer and the core flow in a diffuser, and in the inlet section of a pipe. Burke[3] appears to be the only one to have made a similar calculation for the flow in a hypersonic nozzle. Following Schlichting the conservation equations will be simultaneously formulated for both the core and boundary layer flows.

In the present case the boundary layer thickness is of the same order as the radius of the nozzle, consequently the effect of transverse curvature, which has been discussed by Durand and Potter,[56] and Michel,[48] must be taken into account. The coordinate system used in the present case is the same as that used in References 48 and 56 and is shown in Figure 1. The analysis will be restricted to a concical expansion nozzle.

The flow is divided into a useful inviscid core and a boundary layer of thickness δ. The mass flow will be computed across the surface S = constant in the boundary layer and the adjoining spherical cap of radius R_c in the inviscid core. If V_e is the component of the core velocity normal to the spherical cap, then the mass flow $\dot{m}$ is given by

$$\dot{m} = \int_0^{\delta} 2\pi\, r\rho u\, dy + \int_0^{\theta_{uc}} \rho_e V_e \cdot 2\pi\, R_c^2 \sin\theta\, d\theta \quad . \tag{1}$$

In general the velocity distribution within the core must be computed by the method of characteristics. The flow through an inviscid conical nozzle will be of a source type, and it will be assumed that even with a boundary layer the core flow behaves as a source flow so that ρ_e and V_e in Equation 1 are constant. There are some indications that this is not too unreasonable an assumption to make.[3]

As in References 48 and 56 the displacement thickness is defined by the relation

$$\int_0^{\delta^*} 2\pi\, r\rho_e u_e\, dy = \int_0^{\delta} 2\pi\, r(\rho_e u_e - \rho u)\, dy \quad . \tag{2}$$

Here u_e, the velocity at the edge of the boundary layer, is

$$u_e = V_e \cos(\theta_w - \theta_{uc}) \tag{3}$$

and since

$$r = R - y\cos\theta_w \tag{4}$$

it follows from Equation 2 that

$$\int_0^{\delta} 2\pi\, r(\rho_e u_e - \rho u)\, dy = 2\pi\rho_e V_e \cos(\theta_w - \theta_{uc}) \left(R\delta^* - \frac{\delta^{*2}}{2}\cos\theta_w\right) \quad . \tag{5}$$

Combining Equations 4 and 5 with 1 the following expression is obtained for $\dot{m}$

$$\dot{m} = 2\pi \rho_e V_e \left[R_c^2 (1 - \cos \theta_{uc}) + \left(R\delta - \frac{\delta^2}{2} \cos \theta_w \right) \cos (\theta_w - \theta_{uc}) \right.$$

$$\left. - \left(R\delta^* - \frac{\delta^{*2}}{2} \cos \theta_w \right) \cos (\theta_w - \theta_{uc}) \right] \quad . \tag{6}$$

In Appendix A it is shown that to a very close approximation Equation 6 can be replaced by the much simpler approximate expression

$$\dot{m} = \pi \rho_e V_e (R - \delta^*)^2 \tag{7}$$

provided that $\theta_w << 1$. This generally is the case; for example, in the University Hot Shot Tunnel $\theta_w = 7.5^o$ and the error introduced by using Equation 7 is of the order of 1% assuming $\delta^*/R \sim 0.25$ and $\delta/\delta^* \sim 2$.

In formulating the momentum equation it will be assumed at the outset that $\theta_w << 1$ so that the velocity distribution across the nozzle will be approximately as shown in Figure 2. In view of the calculation of mass flow above, this assumption appears reasonable. Assuming that the pressure remains constant across the boundary layer application of conservation of momentum to a control volume of length dx (see Figure 2) yields the equation

$$\frac{d}{dx} \left[\int_0^R 2\pi \rho u^2 r dr \right] = - \pi R^2 dp - \tau_w 2\pi R dx \quad . \tag{8}$$

For the case $\theta_w << 1$ the relation between r and y becomes

$$r = R - y \tag{9}$$

and Equation 5 defining the displacement thickness δ^* becomes

$$\delta^* - \frac{\delta^{*2}}{2R} = \overline{\delta^*} = \int_0^R \frac{r}{R} \left(1 - \frac{\rho u}{\rho_e u_e} \right) dr \tag{10}$$

where the subscript e refers to the isentropic core flow. It is in the present case expedient to carry the integration in Equation 10 from the tunnel axis to the wall rather than only across the boundary layer. Since it is assumed that there is a uniform core this change from Equation 5 will not affect the results.

Again as in References 48 and 56 a momentum thickness δ_2 is defined by the relation

$$\int_0^{\delta_2} 2\pi r(\rho_e u_e^2)\, dy = \int_0^{\delta} 2\pi r\rho(u_e u - u^2)\, dy. \tag{11}$$

Changing variables and extending the integral on the right side of Equation 11 across the entire nozzle there results the relation

$$\delta_2 - \frac{\delta_2^2}{2R} = \overline{\delta_2} = \int_0^{R} \frac{\rho u}{\rho_e u_e}\left(1 - \frac{u}{u_e}\right)\frac{r}{R}\, dr. \tag{12}$$

After some simple algebraic manipulation it is possible to show that

$$\int_0^{R} \rho u^2 r\, dr = -\rho_e u_e^2 R\,\overline{\delta_2} - R\rho_e u_e^2\,\overline{\delta^*} + \frac{R^2}{2}\rho_e u_e^2 \tag{13}$$

so that the momentum Equation 8 becomes

$$\frac{d}{dx}(\rho_e u_e^2 R\,\overline{\delta_2}) + \frac{d}{dx}(R\rho_e u_e^2\,\overline{\delta^*}) - \frac{d}{dx}\left(\frac{R^2}{2}\rho_e u_e^2\right) = \frac{R^2}{2}\frac{dp}{dx} + R\tau_w \quad . \tag{14}$$

From Equation 7 for the conservation of mass it follows that

$$\frac{d}{dx}(\rho_e u_e R\,\overline{\delta^*}) = \frac{1}{2}\frac{d}{dx}(\rho_e u_e R^2). \tag{15}$$

Combining Equations 14 and 15 the momentum equation becomes

$$\frac{d\overline{\delta_2}}{dx} + \overline{\delta_2}\left[\frac{\overline{H} + 2}{u_e}\frac{du_e}{dx} + \frac{1}{\rho_e}\frac{d\rho_e}{dx} + \frac{1}{R}\frac{dR}{dx}\right] = \frac{c_f}{2} + \frac{R}{2\rho_e u_e^2}\left(\frac{dp}{dx} + \rho_e u_e \frac{du_e}{dx}\right) \quad . \tag{16}$$

If the core flow is isentropic, which implies either frozen or equilibrium flow, then

$$\frac{dp}{dx} = - \rho_e u_e \frac{du_e}{dx} \tag{17}$$

so that Equation 16 becomes

$$\frac{d\overline{\delta_2}}{dx} + \overline{\delta_2}\left[\frac{\overline{H} + 2}{u_e}\frac{du_e}{dx} + \frac{d}{dx}(\ln \rho_e R)\right] = \frac{c_f}{2}, \tag{18}$$

where $\overline{H} = \overline{\delta^*}/\overline{\delta_2}$. Thus, with an isentropic core the integral momentum equation for the entire nozzle reduces to the same form as the boundary layer momentum integral equation. This result is identical with that of Schlichting[48] for the incompressible flow in an axially symmetric diffuser. It should be observed that since the flow in question is turbulent, the fluid velocities used in formulating Equations 18 and 7 are average values. The effect of transverse curvature enters through the fact that Equation 18 is in terms of the quantities $\overline{\delta_2}$ and $\overline{H}$ rather than in terms of the usual parameters δ_2, δ^* and $H = \frac{\delta^*}{\delta_2}$.

If h_o is total average enthalpy then application of conservation of energy to the control volume in Figure 2 yields.

$$\frac{d}{dx}\left[\int_0^R 2\pi r \rho u h_o dr\right] = 2\pi R q_w, \tag{19}$$

where q_w is the heat flux per unit area from the wall to the fluid. Definition of an energy thickness δ_3 by

$$\int_0^{\delta_3} 2\pi r \rho_e u_e h_{oe} dy = \int_0^{\Delta} 2\pi r \rho u (h_o - h_{oe}) \tag{20}$$

as is also done in Shapiro,[57] leads to the relation

$$\delta_3 - \frac{\delta_3^2}{2R} = \overline{\delta_3} = \int_0^R \frac{\rho u}{\rho_e u_e} \frac{r}{R} \left(\frac{h_o}{h_{oe}} - 1 \right) dr \quad . \tag{21}$$

In Equation 20 Δ is the thickness of the thermal boundary layer. Using Equation 21 and the continuity equation, and assuming an adiabatic core flow so that h_{oe} remains constant. Equation 19 can be recast into the form

$$\frac{d\overline{\delta_3}}{dx} + \overline{\delta_3} \frac{d}{dx} (\ln \rho_e u_e R) = \frac{q_w}{\rho_e u_e h_{oe}} \quad . \tag{22}$$

Equation 22, which is valid for the entire nozzle, has the same form as the boundary layer energy integral equation given by Shapiro.[57]

B. Discussion of the Nozzle Integral Equations

Determination of the nozzle flow now requires simultaneous solution of Equations 7, 18, and 22 for the conservation of mass, momentum and energy in order to determine the displacement and momentum thicknesses δ^* and δ_2. Equations 18 and 22 are closely related to the conventional boundary layer integral equations; however, while u_e, the external velocity, is usually known the nozzle problem is complicated by the fact that the variation of u_e is itself dependent upon the solution of Equations 18 and 22 for u_e must satisfy Equation 7 for the conservation of mass.

Methods of solving the turbulent boundary layer integral equations are discussed in References 1, 46, 48, 49, 51, 57, and 58. Because the relation between the turbulent transport of momentum and energy and the average fluid velocity is not yet understood, all of these methods require a number of empirical assumptions, which are discussed below.

A key assumption in many boundary layer studies is that the velocity profile at any point in the boundary layer can be described by a universal relation of the form

$$\left(\frac{u}{u_e} \right) = f\left(\frac{y}{\delta} \right). \tag{23}$$

This assumption is verified experimentally for fully developed incompressible pipe flow and for the incompressible turbulent boundary layer on a flat plate. It is found that boundary layer and pipe velocity profiles are well represented by the relation[58]

$$\frac{u}{u_e} = \left(\frac{y}{\delta}\right)^{\frac{1}{n}} \tag{24}$$

where n varies from approximately 5-12 with increasing Reynolds number. A universal logarithmic velocity profile valid over a wide range of Reynolds number also can be derived starting from the Prandtl mixing length hypothesis or from the VonKarman similarity hypothesis.[58] Because of its greater simplicity, the power law profile of Equation 24 has been used in most investigations. The fact that Equation 24 is equally valid for flat plate and pipe flows means that this relation is unaffected by the transverse curvature of axisymmetric nozzle boundary layers.

Even though Equation 24 is strictly valid only for pipe or flat plate incompressible flows, many investigators have used this velocity profile in the study of compressible turbulent boundary layers with a favorable pressure gradient.[1, 4, 48, 57] An alternative assumption is based on the application of the Stewartson Transformation to the turbulent boundary layer momentum integral equations. In that case Cohen[63] and Reshotko and Tucker[49] have assumed that the velocity profile satisfies Equation 24 in the transformed variables. The validity of this approach is in part supported by Spence's[64] study of boundary layer data. Most boundary layer studies make the assumption that favorable pressure gradients do not have a major effect upon the boundary layer velocity distribution.

In incompressible flow the momentum and displacement thicknesses can be determined as a function of the boundary layer thickness δ once the velocity profile is known. In compressible boundary layers, on the other hand, a knowledge of the density and therefore the enthalpy variation is also required. Thus the

energy and momentum equations are coupled and must be solved simultaneously. One approach to this problem which eliminates the need to directly solve the energy equation is to use the Crocco relation

$$\frac{h_o - h_w}{h_{oe} - h_w} = \frac{u}{u_e} \tag{25}$$

between the total enthalpy and velocity variation across the boundary layer. The Crocco relation is strictly valid only when free stream and wall properties are constant and when the laminar Prandtl number is equal to one.[61] Equation 25 implies that thermal and velocity boundary layer thicknesses are equal. Even when free stream pressure is variable and when $Pr \neq 1$ the Crocco relation has been used in the modified form[4, 46, 65]

$$h = h_w + (h_{aw} - h_w)\frac{u}{u_e} - (h_{aw} - h_e)\left(\frac{u}{u_e}\right)^2, \tag{25a}$$

where the recovery enthalpy, h_{aw}, is given by

$$h_{aw} = h_e + P_r^{1/3}(h_{oe} - h_e). \tag{26}$$

Burke[52] has advanced the argument, similar to that given by Lees[60] for laminar flow, that for $h_w/h_{aw} << 1$ the effects of favorable pressure gradients upon boundary layer behavior will be small so that then it is not unreasonable to extend the use of the Crocco relation.

An alternative approach, which was used by Bartz,[47] is to actually solve the energy integral equation. Thus Bartz assumed a power law of the form

$$\frac{T_o - T_w}{T_{oe} - T_w} = \left(\frac{y}{\Delta}\right)^{\frac{1}{7}} \tag{27}$$

for the total temperature variation across the boundary layer, where Δ is the thickness of the thermal boundary layer. Clearly Equation 27 is closely related

to the Crocco relation. In order to solve the energy Equation 22 a relation between the wall heat flux and other boundary layer parameters is required. For this purpose Bartz used the modified Reynolds analogy.

$$St = \frac{q_w}{\rho_e u_e (h_{aw} - h_w)} = \frac{c_f/2}{\left(\frac{\Delta}{\delta}\right)^{1/7} Pr^{0.46}} \tag{28}$$

for the case in which thermal and velocity boundary layer thickness are not equal. Even when the Crocco relation is used it still is necessary to use some form of the Reynolds analogy to compute wall heat transfer. Other authors[5, 59] have found that the incompressible form of the Reynolds analogy with a correction factor to account for diffusion effects remains valid so that

$$St = \frac{c_f}{2} Pr^{-2/3} \left[1 + (Le^{2/3} - 1) \frac{(\alpha_e - \alpha_w)}{(h_{aw} - h_w)} h_A{}^o\right]. \tag{29}$$

Equation 29 is based on the assumption that air may be approximated as a binary mixture of atoms and molecules. α is the mass fraction of atoms, $h_A{}^o$ is the heat of formation per unit mass of atoms, and Le is the Lewis number. If Le = 1 or if $\alpha_e = \alpha_w = 0$ as is to be expected in the hypersonic portion of a wind tunnel nozzle, then Equation 29 indicates that diffusion has no effect upon the Reynolds analogy.

For the solution of the momentum Equation 18 and for the calculation of heat transfer from Equation 29 a relation between the skin friction coefficient and the parameters of the flow is required. Since the mechanisms of turbulent transport are not yet understood it is necessary to introduce an empirical skin friction law, and this fact introduces the major uncertainty into the results of turbulent boundary layer calculations.[4]

Measurements of fully developed pipe flows have provided the basis for the empirical power law expressions for the friction coefficient.[58, 61] In the incompressible case it has been found that experimental results for smooth pipes could

be correlated over a limited Reynolds number range by a relation of the form

$$c_f = \frac{T_w}{\frac{1}{2}\rho_e u_e^2} = A\left(\frac{\rho_e u_e R}{\mu_e}\right)^{-m}, \tag{30}$$

where u_e is the velocity at the center of the pipe and R is the pipe radius. What is significant is that these laws remain valid for boundary layers provided that R and u_e are replaced by the boundary layer thickness and the free stream velocity. Prandtl[61] has shown that Equation 30 leads to a velocity distribution of the form

$$\left(\frac{u}{u_e}\right) = \left(\frac{y}{\delta}\right)^{\frac{m}{2-m}} \tag{31}$$

which of course has the same form as Equation 24. By substituting Equations 30 and 31 into the momentum integral equation for a flat plate turbulent boundary layer it is possible to express the friction coefficient in the form

$$c_f = A^{\frac{1}{m+1}}\left[\frac{(m+1)(m+2)}{m(2-m)}\right]^{-\frac{m}{m+1}}\left(\frac{u_e x}{\nu_e}\right)^{-\frac{m}{m+1}}, \tag{32}$$

where x is the distance from the leading edge of the plate and it is assumed that the boundary layer is turbulent over the entire plate. In the case of the well known Blasius law with A = .0466 and m = 1/4 this leads to the result

$$c_f = .0592\left(\frac{u_e x}{\nu_e}\right)^{-\frac{1}{5}}. \tag{33}$$

For a flat plate it also can be shown from Equation 31 that

$$\frac{\delta_2}{\delta} = \frac{m(2-m)}{2(m+2)}$$

so that the friction coefficient can be expressed in the form

$$c_f = A\left[\frac{m\,(2-m)}{2\,(m+2)}\right]^m \mathrm{Re}_{\delta_2}^{-\frac{1}{4}} \tag{34}$$

where

$$\mathrm{Re}_{\delta_2} = \frac{\rho_e u_e \delta_2}{\mu_e}.$$

Since Equation 30 has been found to apply both to pipe flow and flat plate boundary layers its validity should in no way be affected by the transverse curvature effect. On the other hand the derivations of the friction law in terms of the distance x from the leading edge or the momentum thickness are based on the assumption of two dimensional boundary layer flow, and therefore may no longer be applicable when $\delta/R \sim O(1)$. In Appendix B it is shown that in this case the relation between c_f and x should, to first order in δ/R, take the form

$$c_f = c_{f_P}\left[1 - k_4 \frac{x}{R}\left(\frac{u_e x}{\nu_e}\right)^{-\frac{m}{m+1}}\right] \tag{34}$$

where the constant k_4 is defined in Appendix B, and c_{f_P} is the plane value of the friction coefficient given by Equation 33. Numerous authors have used the flat plate relations in the analysis of nozzle boundary layers[4, 5, 46] and of course this procedure will be valid if the boundary layers are thin compared to the radius of curvature. On the other hand Michel[48] in his nozzle boundary layer study has taken transverse curvature into account by starting with a friction law based on the boundary layer thickness δ.

Incompressible skin friction laws also have been derived starting from either the Prandtl mixing length hypothesis or the VonKarman similarity hypothesis. The resultant friction laws, the best known of which are perhaps the Prandtl and the VonKarman Schoenherr relations, are logarithmic in form, and are valid over a much larger Reynolds number range than the power laws.[58, 61]

Remarkably it has been found that the incompressible friction laws can be extended to compressible flows if the density and viscosity are evaluated at an appropriate reference temperature.[5, 61, 66, 68] Frequently the Eckert reference temperature

$$T^* = 0.50\,(T_e + T_w) + 0.22\,(T_{aw} - T_e) \tag{35}$$

has been used, or in the case of variable specific heat and dissociation Hayes and Probstein[5] suggest evaluation of ρ and μ at a temperature corresponding to the reference enthalpy

$$h^* = 0.50\,(h_e + h_w) + 0.22\,(h_{aw} - h_e). \tag{36}$$

The situation is somewhat different for a highly cooled stagnation point boundary layer. In this case, since the free stream Mach numbers are small and since the major part of the temperature change is confined to the laminar sublayer Rose, et al,[67] suggest use of the incompressible skin friction formula.

Compressible skin friction formulas also have been derived using the Prandtl mixing length hypothesis. Van Driest has used this method to derive his well known skin friction formula[50] for a perfect gas and others have extended his work to include the effects of dissociation.[4, 59] Dorrance[59] also has computed a friction coefficient for dissociated turbulent boundary layers starting with the Prandtl hypothesis. The Van Driest and Dorrance formulae are considerably more complex than the power laws, though perhaps applicable over a wider Reynolds number range.

It is clear that a large number of skin friction formulas are available. Enkenhus and Maher[4] have calculated the heat transfer at a nozzle throat using several different friction laws and found heat transfer rates ranging from 4200 BTU/ft^2 sec to 12,300 BTU/ft^2 sec indicating the importance of the choice of friction coefficient. The best agreement with experimental results seems to be obtained when the reference enthalpy concept is used in conjunction with either a power law or one of the incompressible logarithmic formulas, or if the

Van Driest or Dorrance friction laws are used.[4, 46, 48] In general it is assumed that the friction laws are not affected by a favorable pressure gradient. Variation of free stream properties is taken into account by using local values of velocity, density and viscosity to evaluate the Reynolds number.

Solution of the momentum integral equation also requires a knowledge of H, the ratio of displacement to momentum thickness. In boundary layers with adverse pressure gradients, the velocity profiles do not obey the power law (Equation 23) and in the case of incompressible flow Von Doenhoff and Tetervin have shown that H acts as a form parameter which determines the nature of the velocity profile. Thus one approach to a solution of the boundary layer integral equations is to consider H and δ_2 as the basic variables and to use an empirical equation relating H, δ_2, shear stress and pressure gradient in conjunction with the momentum equation in order to obtain H and the displacement thickness.

With a favorable pressure gradient, such as will be the case in a wind tunnel nozzle most investigators have assumed a velocity profile of the form given by Equation 24. In incompressible flow H_i then is determined by the definition of δ^* and δ_2, its value being dependent on n in Equation 24, and hence on the Reynolds number. The subscript i here denotes the incompressible value of H. In compressible flow H also depends upon the variation of the density across the boundary layer. With increasing free stream Mach number M_∞ and recovery enthalpy there is a large increase of the displacement thickness δ^* relative to the momentum thickness so that H increases drastically. Most investigators[46, 48, 62] have used the modified Crocco relation (Equation 25a) to compute ρ and hence the form parameter H. Using this approach Michel[68] has computed and tabulated H for a perfect gas with constant specific heats over the range

$$0 \leq \left(\frac{h_{aw}}{h_e}\right) - 1 \leq \infty; \qquad 0 \leq \frac{h_w}{h_{aw}} \leq 1.5$$

for n = 5 (Equation 23) and $H_i = 1.4$, and for this case also gives the approximate formula

$$H = 1.4 + 2.222\left(\frac{h_{aw}}{h_e} - 1\right) + 1.222\,\frac{h_w - h_{aw}}{h_e} + \delta H, \tag{37}$$

where δH is a correction factor which depends upon h_w/h_{aw} and $(h_{aw}/h_e - 1)$. For a perfect gas with constant specific heats Sivells gives the formula

$$H = H_i\left(\frac{T_w}{T_e}\right) + \left(\frac{T_{aw} - T_e}{T_e}\right) \tag{37a}$$

which agrees with experiment up to Mach numbers of 5.0. Equations 37 and 37a appear to be in reasonable agreement, and with the exception of the factor δH, are identical when $T_w = T_e$.

In Reference 57 values of H are tabulated for $H_i = 1.286$, $n = 7$ and up to $M_\infty = 10$. Corrections for real gas effects are discussed by Michel.

The form factor appearing in Equation 18 is

$$\overline{H} = \frac{\overline{\delta^*}}{\overline{\delta_2}}$$

rather than the usual factor

$$H = \frac{\delta^*}{\delta_2}$$

The effect of transverse curvature upon H has been investigated by Michel,[48] who found that to a reasonable degree of approximation

$$H \cong \overline{H}$$

for turbulent boundary layers with a cold wall. In the extreme case of $\delta/R \cong 1$ and $h_w = h_{aw}$ Michel found that $\overline{H}/H = 1.05$.

C. Approximate Hypersonic Solutions of the Nozzle Momentum Integral Equation

Solution of the boundary layer integral equations usually requires numerical integration. Under certain conditions, such as when the core flow is hypersonic, the equations can be sufficiently simplified to permit closed form integrations. One cannot expect the resulting solutions to agree exactly with experiment; however, the solutions do provide a guide to the interpretation of experimental data in that they show how key parameters such as the free stream Mach and Reynolds numbers influence the boundary layer behavior. Closed form solutions have, for example, been found by Cohen,[63] who applied the Stewartson transformation to the boundary layer integral equations, and by Burke,[52] who utilized assumptions valid when the core flow is hypersonic. The assumptions utilized by Burke are used below to simplify the complete nozzle integral momentum equation (Equation 18). The effect of using various forms of the skin friction law are then explored.

The analysis starts from the momentum equation

$$\frac{d\overline{\delta_2}}{dx} + \overline{\delta_2}\left[(\overline{H} + 2)\frac{1}{u_e}\frac{du_e}{dx} + \frac{d}{dx}(\ln \rho_e R)\right] = \frac{c_f}{2} \quad , \tag{18}$$

and the continuity equation

$$\dot{m} = \pi \rho_e u_e (R - \delta^*)^2 \quad . \tag{7}$$

It is assumed that the inviscid core flow is hypersonic so that

$$\frac{(\gamma - 1)}{2} M_e^2 >> 1 \tag{38}$$

and that

$$\begin{aligned} T_w &\sim T_e \\ T_w, T_e &<< T_o \quad . \end{aligned} \tag{39}$$

A futher assumption is that the fluid behaves as a perfect gas at the low static temperature of the hypersonic free stream so that Reece's approximate flow equations (see Appendix C) can be used. The coefficients of $\overline{\delta_2}$ and c_f can then be simplified sufficiently to make an explicit solution of Equation 18 possible, as is shown below.

Since the free stream behaves as a perfect gas it follows that

$$\frac{h_o}{c_{pe} T_e} = 1 + \frac{\gamma - 1}{2} M_e^2 \quad . \tag{40}$$

Since

$$u_e = \sqrt{\gamma R T_e}\, M_e \tag{41}$$

combination of Equations 40 and 41 yields

$$\frac{1}{u_e}\frac{du_e}{dx} = \frac{2}{M_e}\frac{dM_e}{dx}\left[\frac{1}{(\gamma - 1) M_e^2} + O\left(\frac{1}{M_e^4}\right)\right] \quad . \tag{42}$$

As long as the free stream behaves as a perfect gas

$$\rho_e = \rho_o\, F(p_o, h_o)\left[1 + \frac{\gamma - 1}{2} M_e^2\right]^{-\frac{1}{\gamma - 1}} \quad , \tag{43}$$

where $F(p_o, h_o)$ is a function of the stagnation conditions. Thus for fixed stagnation conditions

$$\frac{1}{\rho_e}\frac{d\rho_e}{dx} = \frac{d(\ln \rho_e)}{dx} = -\frac{2}{\gamma - 1} \cdot \frac{1}{M_e}\frac{dM_e}{dx}\left[1 + O\,\frac{1}{(\gamma - 1) M_e^2}\right] \quad . \tag{44}$$

If it is assumed that the diverging part of the nozzle is conical $R = \theta_w x$. Therefore

$$\frac{d(\ln R)}{dx} = \frac{1}{R}\frac{dR}{dx} = \frac{1}{x} \quad . \tag{45}$$

As shown in Appendix C, the Mach number M_e and the effective core area are related by

$$A_{eff} = f_1 (p_o, h_o) A_t \cdot \frac{1}{M_e} \left[\frac{2}{\gamma + 1} \left(1 + \frac{\gamma - 1}{2} M_e^2 \right) \right]^{\frac{\gamma + 1}{2(\gamma - 1)}} \tag{C-5}$$

where $f_1 (p_o, h_o)$ is a function of the stagnation conditions and is discussed in Appendix C. It now follows that for fixed A_t and stagnation conditions

$$\frac{1}{A_{eff}} \frac{d A_{eff}}{dx} = \frac{2}{\gamma - 1} \frac{1}{M_e} \frac{dM_e}{dx} \left\{ 1 + O\left[\frac{1}{(\gamma - 1) M_e^2} \right] \right\}. \tag{46}$$

If the modified Crocco relation holds it follows that, since $h_w << h_o$, the maximum enthalpy within the boundary layer is only about $1/4\ h_o$. Consequently it should not be too unreasonable to use Equation 37, developed for a perfect gas with constant specific heats, for H. Assuming $h_w = h_e$ and $P_r = 1$, Michel's expression reduces to

$$H = 1.4 + \frac{\gamma - 1}{2} M_e^2 \simeq \frac{\gamma - 1}{2} M_e^2 \quad . \tag{47}$$

Further as mentioned previously $H \sim \overline{H}$.

Introducing these results the momentum equation becomes

$$\frac{d\overline{\delta_2}}{dx} + \overline{\delta_2} \left[\frac{(\gamma - 3)}{2} \frac{1}{A_{eff}} \frac{d A_{eff}}{dx} + \frac{1}{x} \right] = \frac{c_f}{2} \tag{48}$$

and there remains the problem of evaluating c_f and $1/A_{eff} \cdot d A_{eff}/dx$. Since $A_{eff} = \pi (R - \delta^*)^2$ it follows that

$$\frac{1}{A_{eff}} \frac{d A_{eff}}{dx} = \frac{2 \left(\theta_w - \frac{d\delta^*}{dx} \right)}{\theta_w x - \delta^*} \quad . \tag{49}$$

Results of boundary layer calculations[4, 46] indicate that, at least over a limited distance, $\delta^* \sim x$. Assuming this to be the case

$$\frac{1}{A_{eff}} \frac{d A_{eff}}{dx} \cong \frac{2}{x} \tag{50}$$

so that the momentum equation becomes

$$\frac{d\overline{\delta_2}}{dx} - \frac{(2 - \gamma)}{x} \overline{\delta_2} = \frac{c_f}{2} \quad . \tag{51}$$

The form which the solution of Equation 51 takes now depends upon c_f.

One possibility is to use the flat plate type of power law combined with the reference temperature concept so that

$$\frac{\tau_w}{\rho^* u_e^2} = A_s \left(\frac{\rho^* u_e x}{u^*} \right)^{-s} \quad . \tag{52}$$

From Equation 52 it follows that

$$\frac{c_f}{2} = \frac{\tau_w}{\rho_e u_e^2} = \frac{\rho^*}{\rho_e} A_s \left(\frac{\rho^* u_e x}{u^*} \right)^{-s} \tag{53}$$

and this is the skin friction law used by Burke.[52] Since $u_e \sim \sqrt{2h_o}$, Equation 53 can be expressed in the form

$$\frac{c_f}{2} = A_s \left(\frac{\rho^*}{\rho_e} \right) \left(\frac{\rho^*}{\rho_e} \right)^{-s} \left(\frac{\rho_e}{\rho_o} \right)^{-s} \left(\frac{\mu_o}{\mu^*} \right)^{-s} \left(\frac{\rho_o \sqrt{2h_o}\, x}{\mu_o} \right)^{-s} \quad . \tag{54}$$

Once again since $h^* \leq \frac{1}{4} h_o$ in the hypersonic part of the nozzle it appears reasonable to assume that

$$\frac{T_e}{T^*} \cong \frac{h_e}{h^*} \quad .$$

Now $h^* = 0.50\,(h_e + h_w) + 0.22\,(h_{aw} - h_e)$, and when, $h_e, h_w << h_{aw} \sim h_o$ it is approximately true that

$$h^* \cong \beta h_o \tag{55}$$

where β is a constant. Thus it also follows that

$$\frac{T_e}{T^*} \cong \frac{h_e}{h^*} = \frac{h_e}{\beta h_o} = \frac{1}{\beta E} \tag{56}$$

where from Equation C-3 it follows that

$$E = \frac{h_o}{h_e} \cong \frac{\gamma - 1}{2} M_e^2 \quad . \tag{57}$$

Further for given stagnation conditions T_o/T^* will be constant. Now it is assumed that $\mu \sim T^{\omega}$. Also since the pressure across the boundary layer is constant

$$\frac{\rho^*}{\rho_e} = \frac{T_e}{T^*}$$

and, hence, using the above results

$$\frac{c_f}{2} = A_s \left(\frac{T_o}{T^*}\right)^{-\omega s} \left[F(p_o, h_o)\right]^{-s} \left(\frac{\rho_o \sqrt{2\,h_o}}{\mu_o}\right)^{-s} x^{-s}\, E^{(s-1)\,+\,\frac{s}{\gamma - 1}}\, \beta^{s-1} \quad . \tag{58}$$

From Equation C-5, E and the effective core area are related by

$$E = \frac{\gamma - 1}{2} M_e^2 = \frac{\left(\frac{\gamma - 1}{2}\right) (A_{eff}/A_t)^{\gamma - 1}}{f_1^{\gamma - 1} \left(\frac{\gamma - 1}{\gamma + 1}\right)^{\frac{\gamma + 1}{2}}} \quad . \tag{59}$$

Now once again using the assumption that $\delta^* \sim x$ so that $\delta^* = Sx$ where S = a constant, Equation 59 yields the following relation between E and x:

$$E = \frac{\left(\frac{\gamma - 1}{2}\right)(\theta_w - S)^{2(\gamma - 1)}}{f_1^{(\gamma - 1)}\left(\frac{\gamma - 1}{\gamma + 1}\right)^{\frac{\gamma + 1}{2}}} \left(\frac{x}{r_t}\right)^{2(\gamma - 1)} \quad . \tag{60}$$

Combining the above results the momentum equation becomes

$$\frac{d\overline{\delta_2}}{dx} - \frac{(2 - \gamma)}{x}\overline{\delta_2} = \psi_1 (p_o, h_o)\left(\frac{r_t}{L}\right)^{-s}\left(\frac{x}{r_t}\right)^{2(\gamma - 1)(s - 1) + s} \tag{61}$$

where ψ_1 is a dimensionless function given by

$$\psi_1 (p_o, h_o) = A_s \left(\frac{T_o}{T^*}\right)^{-\omega s}\left[F (p_o, h_o)\right]^{-s}\left(\frac{\rho_o \sqrt{2 h_o}\, L}{\mu_o}\right)^{-s} \beta^{s - 1} \times$$

$$\left[\frac{\left(\frac{\gamma - 1}{2}\right)(\theta_w - S)^{2(\gamma - 1)}}{f_1^{(\gamma - 1)}\left(\frac{\gamma - 1}{\gamma + 1}\right)^{\frac{\gamma + 1}{2}}}\right]^{(s - 1) + \frac{s}{\gamma - 1}} , \tag{62}$$

and where L is some characteristic dimension such as the nozzle length.

Integration of Equation 61 is meaningful only over that part of the nozzle for which the hypersonic approximation is applicable. It will now be assumed that $\overline{\delta_2} = \overline{\delta_{2R}}$ at some position x_R downstream of the throat, where the hypersonic assumptions first become valid.

If the pressure gradient term in Equation 61 is arbitrarily neglected the equation yields the following for $\overline{\delta_2}/x$:

$$\frac{\overline{\delta_2}}{x} = \frac{\overline{\delta_{2R}}}{x} + \frac{\psi_1\left(\frac{r_t}{L}\right)^{-s}}{2(\gamma - 1)(s - 1) + s + 1}\left[\left(\frac{x}{r_t}\right)^{-\ell} - \left(\frac{x_R}{x}\right)\left(\frac{x_R}{r_t}\right)^{-\ell}\right] \tag{63}$$

where $\ell = 2(\gamma - 1)(1 - s) - s$. This solution is often called the flat plate solution, and the only justification for dropping the pressure gradient term is that the form of the resulting solutions often agree with experimental results. Now if

$$\frac{\overline{\delta_{2R}}}{x} << \frac{\overline{\delta_2}}{x} \quad , \qquad \left(\frac{x_R}{x}\right)^{1 - \ell} << 1$$

the flat plate solution becomes approximately

$$\frac{\overline{\delta_2}}{x} \cong \frac{\psi_1 \left(\frac{r_t}{L}\right)^{-s}}{2(\gamma - 1)(s - 1) + s + 1} \left(\frac{x}{r_t}\right)^{-\ell} \quad . \tag{64}$$

Equation 64 thus implies that the major portion of the boundary layer development has occurred in the hypersonic section of the nozzle. From Equation 47 it follows that $\delta_2 << \delta^*$ when the core flow is hypersonic. Thus even when $\delta^*/R \sim O(1)$,

$$\overline{\delta_2} = \delta_2 \left(1 - \frac{\delta_2}{2R}\right) \cong \delta_2 \quad . \tag{65}$$

From Equations 64, 61, and 53 it follows that the flat plate solution can be expressed in the form

$$\frac{\overline{\delta_2}}{x} \cong \frac{\delta_2}{x} = \frac{c_f/2}{2(\gamma - 1)(s - 1) + s + 1} = \frac{A_s \left[\beta \frac{\gamma - 1}{2}\right]^{s + \omega s - 1}}{2(\gamma - 1)(s - 1) + s + 1} \frac{M_e^{2(s + \omega s - 1)}}{Re_x^{s}} \quad , \tag{66}$$

and from Equation 47 it follows that

$$\frac{\delta^*}{x} = \frac{A_s \frac{\gamma - 1}{2} \left(\beta \frac{\gamma - 1}{2}\right)^{s + \omega s - 1}}{2(\gamma - 1)(s - 1) + s + 1} \frac{M_e^{2s(1 + \omega)}}{Re_x^{s}} \quad . \tag{67}$$

Equation 67 was originally derived by Burke;[52] however, he did not take into account the upstream boundary conditions and the effect of the boundary layer upon the core flow. The form of Equation 67 is in agreement with the experimental

coorelation formulas developed by several authors for the hypersonic nozzle boundary layer.[52, 53, 74] Equation 67 is essentially a local similarity solution and implies that the upstream history of the boundary layer is not important. In view of the many approximations needed to derive the above solution it is surprising that it should actually have the same form as the experimental correlations.

If the pressure gradient term in Equation 61 is retained the solution takes the form

$$\frac{\overline{\delta_2}}{x} = \frac{\delta_{2R}}{x_R}\left(\frac{x}{x_R}\right)^{1-\gamma} + \frac{\psi_1\left(\frac{r_t}{L}\right)^{-s}}{1+\ell-\gamma}\left(\frac{x}{r_t}\right)^{-\ell}\left[\left(\frac{x}{x_R}\right)^{1+\ell-\gamma} - 1\right], \tag{68}$$

and it can be seen that the solution (Eq. 68) is quite different from the flat plate solution (Eq. 63). The exponent ℓ and $1 + \ell - \gamma$ is shown in the table below for several values of s which might be expected in the case of a turbulent boundary layer, and for $\gamma = 1.4$.

s	0.20	0.25	0.30	0.35
ℓ	.44	.35	.26	.17
$1 + \ell - \gamma$	.04	-.05	.14	.23

In the range of interest, say $0.20 \leq s \leq 0.3$, $(1 + \ell - \gamma) << 1$ so that Equation 68 may to reasonable accuracy be approximate by

$$\frac{\overline{\delta_2}}{x} \cong \frac{\overline{\delta_{2R}}}{x_R}\left(\frac{x}{x_R}\right)^{1-\gamma} + \psi_1\left(\frac{r_t}{L}\right)^{-s}\left(\frac{x}{r_t}\right)^{-\ell}\ln\left(\frac{x}{r_t}\right)\left(\frac{r_t}{x_R}\right) . \tag{68a}$$

since

$$\lim_{z \to 0}\frac{a^z - 1}{z} = \ln a .$$

There are now no simple arguments by which the effect of boundary layer history can be eliminated. If δ_R/x_R is sufficiently small it may be possible to find an empirical value of the dimensionless reference distance x_R/r_t such that experimental data can be correlated using the formula

$$\frac{\overline{\delta_2}}{x} = \text{const} \frac{M_e^{2(s + \omega s - 1)}}{Re_x^s} \left[\ln\left(\frac{x}{r_t}\right) - \ln\left(\frac{x_R}{r_t}\right) \right] , \tag{69}$$

where $\ln \frac{x_R}{r_t}$ is now essentially an empirical constant. Whether or not Equation 69 will actually result in improved correlations of experimental data is certainly a worthwhile subject for further investigation.

Of course, as stated in Section II-A above, the flat plate skin friction formula is not really applicable to hypersonic nozzles with thick boundary layers. Rather it is more consistent to use a power law based on Re_δ so that

$$\frac{c_f}{2} = B_m \frac{\rho^*}{\rho_e} \left(\frac{\rho^* u_e \delta}{\mu^*} \right)^{-m} \tag{70}$$

To find a solution of the momentum Equation 51 using this friction law it is necessary to find a relation between δ and $\overline{\delta_2}$. From the definition of $\overline{\delta_2}$ in Equation 12 it follows that

$$\overline{\delta_2} = \delta \int_0^1 \frac{\rho}{\rho_e} \frac{r}{R} \left(\frac{u}{u_e} - \frac{u^2}{u_e^2} \right) d\left(\frac{y}{\delta}\right) . \tag{71}$$

Now assuming that

$$\frac{\rho}{\rho_e} \cong \frac{h_e}{h}, \qquad P_r = 1, \qquad \frac{u}{u_e} = \left(\frac{y}{\delta}\right)^{\frac{1}{n}}, \tag{72}$$

and using the Crocco relation, Equation 25a, integration of Equation 71 yields the approximate result

$$\frac{\overline{\delta_2}}{\delta} \cong \frac{1}{nE}\left(1 - \frac{1}{2}\frac{\delta}{R}\right) + \left(O\ \frac{1}{E^2}\ln E\right) \quad . \tag{73}$$

Now Equation 70 for $c_f/2$ can be expressed in the form

$$\frac{c_f}{2} = \psi_2 \left(\frac{r_t}{L}\right)^{-m} \left(\frac{x}{r_t}\right)^{-2(\gamma - 1 - m)} \left(\frac{\overline{\delta_2}/r_t}{1 - \frac{1}{2}\frac{\delta}{R}}\right)^{-m} \tag{74}$$

where

$$\psi_2 = B_m \beta^{m-1} \left(\frac{T_o}{T^*}\right)^{-\omega m} \left(\frac{\rho_o \sqrt{2\, h_o}\, n\, L}{\mu_o}\right)^{-m} \times$$

$$\left[\frac{\frac{\gamma - 1}{2}(\theta_w - S)^{2(\gamma - 1)}}{f_1^{\gamma - 1}\left(\frac{\gamma - 1}{\gamma + 1}\right)^{\frac{\gamma + 1}{2}}}\right]^{\frac{m}{\gamma - 1} - 1} \left[F(p_o, h_o)\right]^{-m} \quad .$$

Now

$$\left(1 - \frac{1}{2}\frac{\delta}{R}\right)^m = 1 - \frac{m}{2}\frac{\delta}{R} + \frac{m(m-1)}{1 \cdot 2} \cdot \frac{1}{4}\left(\frac{\delta}{R}\right)^2 \ldots ,$$

and since m is usually small, for example . 25, the important result follows that the effect of transverse curvature upon c_f will be quite small even when $\delta/R \sim O(1)$.

The momentum equation now becomes

$$\frac{d\overline{\delta_2}}{dx} - \frac{(2 - \gamma)}{x}\overline{\delta_2} = \psi_2 \left(\frac{r_t}{L}\right)^{-m} \left(\frac{x}{r_t}\right)^{-2(\gamma - 1 - m)} \left(\frac{\overline{\delta_2}}{r_t}\right)^{-m} \quad . \tag{75}$$

If the pressure gradient term is ignored Equation 75 has the solution

$$\left(\frac{\overline{\delta_2}}{x}\right)^{m+1} = \left(\frac{\overline{\delta_{2R}}}{x}\right)^{m+1} + \frac{(m+1)\,\psi_2\left(\frac{r_t}{L}\right)^{-m}}{1 - 2(\gamma - 1 - m)} \left(\frac{x}{r_t}\right)^{-m} \times$$

$$\left[\left(\frac{x}{r_t}\right)^{-2(\gamma - 1 - m)} - \left(\frac{x_R}{r_t}\right)^{-2(\gamma - 1 - m)} \left(\frac{x_R}{x}\right)\right] , \tag{76}$$

and if once again $\overline{\delta}_{2R}$ is sufficiently small and

$$\left(\frac{x_R}{x}\right)^{1 - 2(\gamma - 1 - m)} << 1$$

this solution becomes approximately

$$\left(\frac{\overline{\delta_2}}{x}\right) = \left[\frac{(m+1)\,B_m \beta^{m(1+\omega) - m}}{1 - 2(\quad - 1 - m)}\, n^{-m}\right]^{\frac{1}{m+1}} \left(\frac{\gamma - 1}{2}\right)^{\frac{m\omega - 1}{m+1}} \times$$

$$\frac{(M_e^{\,2})^{\frac{m\omega - 1}{m+1}}}{Re_x^{\frac{m}{m+1}}} . \tag{77}$$

If, as in the incompressible case, the coefficient s of the flat plate friction law is related to m by $s = \frac{m}{m+1}$ it is readily shown that the Reynolds and Mach number dependence of $\overline{\delta_2}/x$ indicated by Equations 66 and 77 is identical. This is not surprising since we have shown that the effect of transverse curvature c_f is small.

When the pressure gradient term is retained the solution becomes

$$\frac{\overline{\delta_2}}{x}^{m+1} = \left(\frac{\overline{\delta_{2R}}}{x}\right)^{m+1} \left(\frac{x}{x_R}\right)^{(2-\gamma)(m+1)} +$$

$$\frac{\psi_2 \left(\frac{r_t}{L}\right)^{-m} \left(\frac{x}{r_t}\right)^{-2(\gamma-1)+m}}{\gamma(1-m)-1} \left[\left(\frac{x}{x_R}\right)^{\gamma(1-m)-1} - 1\right] . \qquad (78)$$

For values of m of interest in turbulent flows and with $\gamma = 1.4$, $\gamma(1 - m) - 1$ will be a small number. Hence if $\overline{\delta_{2R}}$ is sufficiently small the solution can be expressed in the approximate form

$$\frac{\overline{\delta_2}}{x} = \left[\psi_2 \left(\frac{r_t}{L}\right)^{-m} \left(\frac{x}{r_t}\right)^{-2(\gamma-1)+m}\right]^{\frac{1}{m+1}} \left(\ln \frac{x}{x_R}\right)^{\frac{1}{m+1}} , \qquad (79)$$

which can also be written

$$\frac{\overline{\delta_2}}{x} = \text{const} \frac{(M_e^2)^{\frac{m\omega-1}{m+1}}}{(Re_x)^{\frac{m}{m+1}}} \left[\ln\left(\frac{x}{r_t}\right) - \ln \frac{x_R}{r_t}\right]^{\frac{1}{m+1}} , \qquad (79a)$$

and this result is very similar to Equation 69 which was obtained using the flat plate friction formula, the only difference being in the exponent of the logarithmic term.

The hypersonic solutions of the momentum and continuity equations found above are relatively insensitive to the transverse curvature effect. The boundary layer thickness correlation formulas (Equations 67, 69, 77, and 79) will be valid only if the major part of the boundary layer development takes place in the hypersonic portion of the nozzle. Because of the usual values assumed by γ,

m, and s, the boundary layer thickness correlation formula obtained with the full momentum equation is the same as the flat plate formula multiplied by a term involving ln (x/x_R). As mnetioned in Section III below, results of boundary layer measurements can be correlated using the flat plate type of formula similar to Equation 67.

The logarithmic term in the more exact solution (Equation 79a) varies very slowly with (x/r_t), and for nozzles with exit Mach numbers between 10 and 20 (x/r_t) varies from approximately 1000-2000. Thus the logarithmic term may be buried in the empirical constants of the experimental flat plate type of correlation formula.

The results above were obtained only after many simplifications and assumptions. The assumption that $\delta^* \approx Sx$ actually gives the solutions the character of a first iteration of the momentum and continuity equations. The solutions found above show that actually $\delta^* \sim x^{1.5}$. Clearly a more precise and simultaneous solution of the momentum and continuity equations is a worthwhile subject for further study. The fact that the hypersonic solutions above, though they may not provide exact quantitative predictions, have the same form as the experimental results appears to indicate that most of the boundary layer development occurs in the hypersonic section of the nozzle.

III. CALCULATION OF HYPERSONIC NOZZLE FLOW USING EMPIRICAL RELATIONS FOR THE BOUNDARY LAYER DISPLACEMENT THICKNESS

An exact integration of the nozzle flow Equations 7, 18, and 22, is a major undertaking which is beyond the scope of the present investigation. Hence, experimental boundary layer thickness correlations have been combined with the continuity Equation 7, in order to calculate the boundary layer and core flow in a conical hypersonic nozzle.

Several investigators[52, 53, 74] have found that experimental measurements of boundary layer thickness at the test section of a hypersonic nozzle can be correlated by an equation of the form

$$\frac{\delta^*}{x} = K \frac{M_e^{\,a}}{Re_x^{\,b}} \quad , \tag{80}$$

which is the same as the flat plate formula found in Section II-C above, or of the form

$$\frac{\delta^*}{x} = \frac{\bar{K}}{\left(\frac{\rho^* u_e x}{\mu^*}\right)^{\lambda}} \quad . \tag{81}$$

$\bar{K}$, K, a, b, and λ are empirical constants, and x is the distance from the nozzle throat to the test section. In Equation 81 the effect of free stream Mach number is taken into account by using the reference enthalpy concept. Burke[52] has shown that Equation 81 correlates experimental results from several sources quite adequately over the Reynolds number range

$$1.5 \times 10^5 \leq Re_x \leq 8 \times 10^6$$

or

$$9 \times 10^3 \leq Re_\delta \leq 3.5 \times 10^5$$

if $\bar{K}$ and λ have the values 0.49 and 0.3 respectively. Burke's empirical constants have been used in the present calculations; however, outside the Reynolds number range for which Equation 81 agrees with experiment, results can only be considered qualitative.

It has been assumed that the flow in the nozzle is in thermodynamic equilibrium, and at relatively high stagnation pressures this assumption is not too unreasonable. Using the results presented by Lukasiewicz[43] a curve corresponding to the case in which 1% of the oxygen in the air freezes out in atomic form has been drawn on a stagnation pressure-density diagram (Figure 3), which also shows the operating domain of the University of Michigan Hot Shot

Tunnel. For stagnation conditions below the 1% freeze out curve the equilibrium assumption should certainly be valid. Since oxygen freeze out nowhere exceeds 10% within the U of M hotshot operating range, the discussion of Lukasiewicz[43] indicates that the effects of nonequilibrium even above the 1% freeze out curve should not be excessive. The above considerations are qualitative; however, a full investigation of the effects of nonequilibrium is beyond the scope of the present investigation.

It now is possible to use the method developed by Burke and Bird[3] to simultaneously calculate the development of the core and boundary layer flows. The details of these calculations are presented in Appendix C.

In a hotshot tunnel stagnation conditions are determined from the arc chamber pressure after firing and from the charging density, which, since energy addition occurs at constant volume, is also the stagnation density. Consequently all results have been presented on stagnation pressure-density diagrams similar to that in Figure 3.

It is of course desirable to put the nozzle calculation results into a universal form which is a function of the stagnation conditions only, but is independent of the detailed nozzle configuration, and to some extent this is possible. However, in the case of the detailed boundary layer thickness calculations not only stagnation conditions but also a factor related to the conical nozzle configuration must be specified. By combining the continuity Equation 7 with the correlation Equation 81 and using Equations C-3 - C-6, Burke and Bird[3] have derived the following equation for the ratio of boundary layer displacement thickness to test section radius:

$$\frac{\delta^*}{R} = \mathcal{J}\left(1 - \frac{\delta^*}{R}\right)^{2\gamma\lambda} F_1(p_o, h_o) \tag{82}$$

where F_1 is a function of stagnation pressure and enthalpy described in Appendix C and where $\mathcal{J}$ is a factor containing the conical nozzle geometry which is given by

$$\mathcal{G} = \frac{1}{\theta_w x^{\lambda}} \left(\frac{\theta_w x}{r_t} \right)^{2\gamma\lambda} = \frac{1}{\theta_w x^{\lambda}} \left(\frac{A_{geom}}{A_t} \right)^{\gamma\lambda} = \left(\frac{x}{R} \right) \left(\frac{R}{r_t} \right)^{2\gamma\lambda} x^{-\lambda} \tag{83}$$

The factor $\mathcal{G}$ provides for some universality in that for a particular stagnation condition, and test gas all nozzle configurations having identical values of $\mathcal{G}$ will have the same value of δ^*/R. In the present case boundary layer calculations have been made for $\mathcal{G} = 363\ (\text{ft})^{-0.3}$ corresponding to

$\theta_w = 7.5^{\circ} = 0.131$ radians

$r_t = 0.05$ in. $= 4.16 \times 10^{-3}$ ft

$x = 72.0$ in. $= 6.00$ ft

$\lambda = 0.3$

The results of the nozzle performance calculations will now be presented in detail.

The range of stagnation conditions of interest in the case of the U of M Hot Shot Tunnel is shown in Figure 3. The stagnation chamber of this tunnel has been designed for a peak pressure of 80,000 psi[73] and this determines the upper boundary of the operating domain. The high temperature boundary is determined by the fact that as T_o increases contamination of the gases from vaporized arc chamber material as well as radiation losses increase above acceptable levels. Calculations have been extended to $T_o = 10,000^{\circ}K$ subject to the assumption that flow contamination is negligible. Indications are that the maximum operating temperature will be less than this value for practical hot shot tunnels.[72] Below a stagnation temperature of $3000^{\circ}K$ test section velocities are too low to be of interest in connection with high speed flight problems. Figure 3 also includes lines of constant stagnation temperature.

In hotshot tunnels energy is added to the test gas at a constant volume. Consequently the energy, E_A, added to the test gas by the arc discharge will be

$$E_A = \rho_o Q_c (e_o - e_i) = \left(\frac{\rho_o}{\rho_R} \right) \left(\frac{e_o}{RT_R} \right) (\rho_R R T_R)\, Q_c \left(1 - \frac{e_i}{e_o} \right) \tag{84}$$

where Q_c is the arc chamber volume and e_o and e_i are the test gas stagnation and initial energies per unit mass. Since $e_i/e_o << 1$ for the domain of interest the curves of $(e_o/RT_R)(\rho_o/\rho_R) = \text{const.}$ correspond to constant values energy addition, E_A. Figure 3 shows that the stagnation pressure depends almost entirely upon E_A and is relatively independent of the charging density. For fixed E_A an increase in charging density simply lowers the stagnation temperature. For $\rho_o/\rho_R > 100$ the thermodynamic data used for Figure 3, as well as for the results to follow was obtained by extrapolating the air Mollier diagram. Results in this region must therefore be regarded with considerable caution.

The results of the boundary layer calculations are presented in Figure 4 in the form of lines of constant $\delta^*/\theta_w x = \delta^*/R$ drawn on a stagnation pressure-density diagram. Figure 4, unfortunately, only is valid for one particular value of the geometrical factor $\mathcal{G}$. It can be seen that δ^*/R decreases with increasing stagnation pressure, a result which is not surprising. What is remarkable is that the curves in Figure 4 pass through a maximum. This means that for a constant stagnation pressure p_o, as the stagnation density ρ_o increases the boundary layer thickness at first increases and then begins to decrease. Consideration of the displacement thickness correlation formula (Equation 80) and Figure 6, which shows contours of constant test section Mach number provides an explanation for this strange result. With p_o constant an increase in ρ_o causes the test section Mach number to increase and this tends to make δ^* increase. On the other hand the static density as well as the Reynold's number also increase with increasing ρ_o, which of course tends to decrease δ^*. The maximum in the boundary layer contours in Figure 4 thus corresponds to the point where these opposing effects balance.

From Equations 82 and 83 it can be seen that

$$\frac{\delta^*}{R} \propto \frac{1}{r_t^{2\gamma\lambda}} \tag{85}$$

or when $\gamma = 1.4$, $\lambda = 0.3$

$$\frac{\delta^*}{R} \propto \frac{1}{r_t^{.84}} \quad .$$

Consequently for a nozzle with fixed length and divergence angle the boundary layer thickness varies almost inversely with the throat radius. This result suggests that it may be possible to experimentally determine λ by measuring the effect of varying the throat radius r_t upon the boundary layer thickness.

The strong dependence of δ^* upon r_t has another interesting consequence. The effective area ratio of a conical nozzle of fixed length and exit area can be increased by decreasing the throat radius r_t. Now because of the relation between r_t and δ^* there is, for a given nozzle and stagnation condition a critical value of throat radius, r_{tc} such that for $r_t < r_{tc}$ the effective nozzle area ratio decreases with decreasing throat radius because of the rapid boundary layer growth. If δ^*/R is not too great Equation 82 becomes approximately

$$\frac{\delta^*}{R} = \mathcal{J} F_1 (p_o, h_o) = \frac{K}{r_t^{2\gamma\lambda}}$$

where K is constant for fixed p_o, h_o, x, θ_w, γ and λ. Now the effective area ratio is given by

$$\frac{A_{eff}}{A_t} = \frac{(R - \delta^*)^2}{r_t^2} = R^2 \left[\frac{1}{r_t} - \frac{K}{r_t^{2\gamma\lambda + 1}} \right]^2$$

and A_{eff}/A_t, considered as a function of r_t, has a maximum when

$$r_t = r_{tc} = [(2\gamma\lambda + 1)K]^{\frac{1}{2\gamma\lambda}} \quad ,$$

and this is the critical throat radius mentioned above. For example, for the nozzle considered above when $p_o = 4000$ atm, $h_o/RT_R = 220$, $r_{tc} = .0123$ in.

and when $p_o = 200$ atm, $h_o/RT_R = 180$, $r_{tc} = .0342$ in. At low stagnation pressures the critical throat radius is thus rather close to the actual values used.

To obtain an overall view of nozzle performance and to determine the range of test section Reynolds numbers encompassed by the domain of stagnation conditions considered here other test section parameters have been computed.

It has been possible to present the variation of test section Mach number in a semi-universal form. Equation C-11 relating Mach number to area ratio can, using Equation C-10, be written in the form

$$M_e = \phi \left(\frac{A_{eff}}{A_t} \right)^{\frac{\gamma - 1}{2}} \tag{86}$$

where the function ϕ is defined by

$$\phi = \left[\left(\frac{\gamma - 1}{\gamma + 1} \right)^{\frac{\gamma + 1}{2(\gamma - 1)}} f_1 (h_o, p_o) \right]^{-\frac{\gamma - 1}{2}} .$$

In the absence of a boundary layer A_{eff}/A_t will be constant so that M_e is directly proportional to the function ϕ, which in that case could be considered a universal Mach number function. Hence contours of ϕ = const. are plotted on a stagnation pressure-density diagram in Figure 5. When boundary layer thickness is appreciable δ^*/R, which can be read from Figure 4, must be known in addition to ϕ in order to determine M_e. Comparison of Figures 3 and 5 shows that M_e decreases with increasing stagnation temperature if the effective area ratio remains constant. This is entirely a real gas effect for in the case of an ideal gas a constant area ratio produces a constant Mach number independent of the stagnation conditions.

The results shown in Figures 4 and 5 have been combined to compute the test section Mach number variation for a nozzle with $\mathcal{J} = 363$ ft$^{-0.3}$. The resultant constant M_e lines are shown in Figure 6. For purposes of comparison several constant Mach number curves have been computed both with and without considering the nozzle boundary layer and the results are shown in Figure 7.

Figure 8 shows constant static pressure contours and in Figure 9 several of these contours are compared to pressure contours computed neglecting the boundary layer. It can be seen that in the present case the static pressure is doubled by the presence of the boundary layer.

Figure 10 shows the variation of test section static temperature with stagnation conditions. Lines of constant static temperature appear to almost coincide with lines of constant stagnation temperature. It should be noted that Reece's[70] perfect gas approximation used in the present calculations is accurate to 1% for $T < 550^{o}K$ therefore, it follows from Figure 10 that the perfect gas approximation remains valid over most of the stagnation conditions of interest.

The variation of static density and the variation of the limiting velocity u_ℓ given by

$$u_\ell = \sqrt{2\, h_o}$$

are shown in Figure 11. In hypersonic flow the free stream velocity u_e is almost equal to u_ℓ. For the Mach number range shown in Figure 6 the free stream velocity u_e is at most 2 1/2% less than the ultimate velocity so that u_ℓ can, for all practical purposes, be regarded as the free stream velocity u_e. Since u_ℓ depends only on the stagnation enthalpy h_o the free stream velocity is essentially independent of the boundary layer development. The free stream density on the other hand will be considerably modified as can be seen from Figure 12, which shows constant density contours computed both with and without the boundary layer. The presence of the boundary layer almost doubles the value of the free stream density.

A comparison of Figures 11 and 6 exposes an interesting aspect of hypersonic nozzle performance. As the free stream velocity, and hence stagnation enthalpy, increase the free stream Mach number actually decreases if the geometric area ratio remains fixed. Thus the flow actually becomes less "hypersonic" as stagnation enthalpy is increased. The Mach number independence principle[5] states that

as $M_e \to \infty$, the flow about bodies becomes independent of M_e and depends only on u_e and ρ_e. Consequently the above effect will not be important insofar as testing is concerned as long as the free stream Mach number remains sufficiently high.

Using the results of the calculations described above the free stream Reynolds number in the present case has been found to lie in the range

$$0.4 \times 10^5 \leq Re_x \leq 4 \times 10^6 \quad .$$

Fortunately this range almost coincides with the range of validity of the empirical formula used to compute boundary layer thickness.

IV. DISCUSSION AND CONCLUSIONS

In the present work integral equations for the flow in a conical hypersonic nozzle with a thick boundary layer have been formulated, and solutions of these equations valid in hypersonic flow have been studied. Burke's method[3] of calculating boundary layer thickness using empirical correlations has been extended over a relatively broad range of stagnation conditions and has been used to compute the effect of boundary layer development upon hypersonic nozzle flow.

The main effect of the nozzle boundary layer is to cause appreciable changes in static pressure, density, and temperature, and to reduce the useful core area of the test section. The free stream velocity depends mainly upon the stagnation enthalpy, and in hypersonic nozzles is unaffected by the boundary layer development.

For a fixed exit diameter and nozzle length, the boundary layer thickness at the nozzle exit varies almost inversely with the throat radius, r_t. This result has two important implications. First as mentioned in Section III, it should be possible to obtain information about the boundary layer thickness correlation formula by measuring the effect of varying throat radius upon the boundary layer thickness. The effective area ratio of a conical nozzle with a fixed length and exit area can be increased by decreasing the throat radius. Now because of

the relation between throat radius and the boundary layer, there is, for a given nozzle, and stagnation condition, a critical value of r_t such that for r_t less than this critical value the effective area ratio of the nozzle will actually decrease because of the rapid boundary layer buildup.

Contours of constant boundary layer thickness drawn on a stagnation pressure-density diagram are found to pass through a maximum. Physically this means that for a fixed nozzle geometry and stagnation pressure, as the stagnation density increases the boundary layer thickness first increases and then begins to decrease. This strange behavior has been explained in Section III by considering the form of the empirical displacement thickness correlation formula.

The boundary layer calculations described in Section III are only as accurate as the boundary layer correlation formula employed and as the approximations to the real gas properties. Over most of the domain of interest the static temperature and nonequilibrium effects seem to be sufficiently small that Reece's approximations are applicable. The range of free stream Reynolds numbers for the particular nozzle considered and the range of validity of the empirical boundary layer thickness correlation formula almost coincide. Mollier charts and cross plotting have been used to compute the results described in Section III, and a certain degree of random error is inherent in this procedure. A precise determination of this error is difficult, though a reasonable estimate would seem to be that the results are valid to an accuracy of $\pm 5\%$ assuming that the boundary layer correlation formula and Reece's approximations are valid.

The incompressible analysis in Appendix B as well as the analysis in Section II show that the transverse curvature of the nozzle boundary layer causes an increase in boundary layer thickness and a decrease in the skin friction coefficient, as compared to a plane boundary layer. The approximate analysis of the momentum equation in Section II shows, however, that in most cases this effect will be negligible even when $\delta^*/R \sim O(1)$, because $\delta_2 << \delta^*$ in hypersonic boundary layers and because the exponent m of the term $(Re_\delta)^m$ in the skin friction law is a relatively small number in turbulent flows.

Using approximations valid in hypersonic flow Burke[52] has shown that the boundary layer momentum equation can be reduced to a relatively simple form. In Section II it is shown that the nozzle integral equations reduce to the same form if it is assumed that $\delta^* \sim x$. Solutions of this equation both with and without the pressure gradient term have been investigated using power skin friction laws based on Re_δ and Re_x. Either friction law leads to essentially the same result. The flat plate solutions, which are obtained when the pressure gradient term is dropped, can be reduced to the form

$$\frac{\delta^*}{x} = \text{const} \frac{M_e^{\,a}}{Re_x^{\,b}}$$

provided the boundary layer thickness at the start of the hypersonic portion of the nozzle is sufficiently small and provided the nozzle is sufficiently long. When the pressure gradient term is retained the corresponding solution has the form

$$\frac{\delta^*}{x} = \text{const} \frac{M_e^{\,a}}{Re_x^{\,b}} \left[\ln \frac{x}{r_t} - \ln \frac{x_R}{r_t} \right]$$

where x_R is an arbitrary distance from the throat where conditions are applied.

In view of the numerous approximations which have been introduced to obtain the above approximate solutions it is remarkable that the form of the flat plate solution is in agreement with the form experimental correlations of boundary layer thickness. This agreement implies that the bulk of the boundary layer growth occurs in the hypersonic portion of the nozzle and this contention is borne out by exact calculations and measurements of boundary layer development.[46, 48] An interesting feature of highly cooled hypersonic boundary layers is that the maximum enthalpy within the boundary layer is only about one quarter of the stagnation enthalpy, assuming that the Crocco relation is valid. Thus real gas effects

will not be important throughout most of the boundary layer, and of course this may be another reason why the approximate solution takes the same form as experimental correlations.

It appears strange that the flat plate rather than the more exact solution seems to provide the best agreement with experiment. There are several possible explanations. The logarithmic term in the exact formula varies very slowly with (x/r_t), and for nozzles with exit Mach numbers between 10-20, x/r_t varies over approximately the range 1000-2000. Consequently it is quite possible that the logarithmic variation is buried in the constant of the empirical correlation formula. In the approximate solution it was assumed, at least for what might be considered a first iteration, that $\delta^* \sim x$. Actually of course δ^* increases more rapidly than this since, approximately, $\delta^* \sim x^{1.5}$. This more rapid boundary layer growth will tend to decrease the free stream pressure gradient and thus provides another possible reason for the success of the flat plate solutions.

There are a number of questions which have not been considered. When the boundary layer is almost as thick as the nozzle there is some question as to whether the boundary layer approximation remains valid and whether the pressure remains constant across the boundary layer. The answers to these questions should depend upon the rate of variation of the core velocity. In the present case both conditions above have been assumed to hold. Effects of chemical nonequilibrium in the core flow and the boundary layer have been neglected. The assumption of equilibrium core flow appears to be valid over most of the domain of stagnation conditions of interest here. Whether or not the boundary layer flow remains in equilibrium is open to question.

In addition to the above the present study suggests a number of further problems which should be investigated in order to gain a fuller understanding of hypersonic nozzle flow.

In view of the above results, the use of the approximate hypersonic nozzle flow integral equations appears as a promising approach to the analysis of

hypersonic nozzle flow, and should be investigated further. A simultaneous solution of the approximate momentum and the continuity equations, without assuming $\delta^* \sim x$, would certainly be desirable. Solutions also should be found using skin friction laws valid over a broader Reynolds number range than the power laws.

A numerical solution of the exact nozzle equations should be obtained at least in a few cases in order to provide a means of evaluating the results of the approximate analysis. Finally an extensive study of existing experimental and theoretical data should be made in order to further check the results of the approximate theory and the experimental correlation formula used for the boundary layer calculations in the present investigation.

REFERENCES

1. Yu, U. N., "A Summary of Design Techniques for Axisymmetric Hypersonic Wind Tunnels," AGARDograph 35, Nov. 1958.

2. Johnson, R. H., "Hypersonic Viscous Effects in Wind Tunnels," ARS Journal, v. 31, pp. 1022-1024, July 1961.

3. Burke, A. F., Bird, K. D., "The Use of Conical and Contoured Expansion Nozzles in Hypervelocity Facilities," from, Advances in Hypervelocity Techniques, Proc. of Second Symposium on Hypervelocity Techniques, Plenum Press, N. Y., pp. 373-424, Mar. 1962.

4. Enkenhus, K. R., Maher, E. F., "The Aerodynamic Design of Axisymmetric Nozzles for High Temperature Air," U. S. Naval Ordnance Lab., White Oak, Md., NAVWEPS Rept. 7395, 5 Feb. 1962.

5. Hayes, W. D., Probstein, R. F., Hypersonic Flow Theory, Academic Press, New York, Capt. 9, 1959.

6. Hilsenrath, J., et al, "Tables of Thermodynamic Properties of Air Including Dissociation and Ionization from 1500°K to 15,000°K," Arnold Engineering Dev. Center, AEDC-TR-59-20, Dec. 1959.

7. Hilsenrath, J., et al, Tables of Thermodynamic and Transport Properties, Pergamon Press, London, 1960.

8. Humphrey, R. L., Neel, C. A., "Tables of Thermodynamic Properties of Air from 90 to 1500°K," Arnold Engineering Dev. Center, AEDC-TN-61-103, Aug. 1961.

9. Treanor, C. E., Logan, J. G., "Thermodynamic Properties of Nitrogen from 2000°K to 8000°K," Cornell Aero. Lab., Rept. BE-1007-A-5, Jan. 1957.

10. Little, W. J., Neel, C. A., "Tables of the Thermodynamic Properties of Nitrogen from 100 to 1500°K," Arnold Engineering Dev. Center, AEDC-TDR-62-170, Sept. 1962.

11. Hilsenrath, et al, "Thermal Properties of Gases," National Bureau of Standards, Circular 564 (1955).

12. Gilmore, F. R., "Equilibrium Composition and Thermodynamic Properties of Air to 24,000°K," The Rand Corp., Santa Monica, Calif., RM-1543, Aug. 1955.

13. Hochstim, A. R., "Gas Properties Behind Shocks at Hypersonic Velocities, III. Tables of Thermodynamical Properties of Air," Convair Div. of General Dynamics Corp., San Diego, Calif., Physics Sec., Rept. ZPh-004, Aug. 1958.

14. Blackwell, F., et al, "Properties of Argon-Free Air," Ramo-Wooldridge Corp., Los Angeles, Calif., Rept. GM-TR-76, Oct. 1956.

15. Goin, K. L., "Mach Tables for Real Gas Equilibrium Flow of Air in Hypervelocity Test Facilities with Total Temperatures to 10,000°K," Sandia Corp., Rept. SCR-288, Mar. 1961.

16. Logan, J. G., Jr., Treanor, C. E., "Tables of Thermodynamic Properties of Air from 3000°K to 10,000°K at Intervals of 100°K," Cornell Aero. Lab., Rept. BE-1007, Jan. 1957.

17. Hansen, C. F., Heims, S. P., "A Review of the Thermodynamic, Transport, and Chemical Reaction Rate Properties of High-Temperature Air," NACA TN 4359, July 1958.

18. Gilmore, J. R., "Additional Values for the Equilibrium Composition and Thermodynamic Properties of Air," The Rand Corp., Rept. RM-2328, 30 Dec. 1959.

19. Chance Vought Research Center Staff, "Thermodynamic Properties of High Temperature Air," Rept. RE-IR-14, 28 June 1961.

20. Feldman, S., "Hypersonic Gas Dynamic Charts for Equilibrium Air," AVCO Research Lab., Research Rept. 40, Jan. 1957.

21. Humphrey, R. L., Little, W. J., Seeley, L. A., "Mollier Diagram for Nitrogen," Arnold Engineering Dev. Center, AEDC-TN-60-83, May 1960.

22. Korobkin, I., Hastings, S. M., "Mollier Charts for Air in Dissociated Equilibrium at Temperatures of 2000°K to 15,000°K," NAVORD Rept. 4446, May 1957.

23. Moeckel, W. E., Weston, K. E., "Composition and Thermodynamic Properties of Air in Chemical Equilibrium," NACA TN 4265, Apr. 1958.

24. Jorgensen, L. H., Baum, G. M., "Charts for Equilibrium Flow Properties of Air in Hypervelocity Nozzles," NASA TN D-1333, Sept. 1962.

25. Yoshikawa, Kenneth K., Katzen, Elliott D., "Charts for Air-Flow Properties in Equilibrium and Frozen Flows in Hypervelocity Nozzles," NASA TN D-693, 1961.

26. Erickson, W. D., Creekmore, Helen S., "A Study of Equilibrium Real-Gas Effects in Hypersonic Air Nozzles, Including Charts of Thermodynamic Properties for Equilibrium Air," NASA TN D-231, 1960.

27. Gibbs, G. J., "Correlation of Real Gas and Perfect Gas Flow Parameters at Hypersonic Velocities in Computing the Free Stream Conditions between Mach 6 and 10," STA Meeting Proc., Vol. II, Apr. 27, 1961.

28. Grabau, M., "A Method of Forming Continuous Empirical Equations for the Thermodynamic Properties of Air from Ambient Temperatures to 15,000°K with Applications," Arnold Engineering Dev. Center, AEDC-TN-59-102, Aug. 1959.

29. Grabau, M., Humphrey, R. L., Little, W. J., "Determination of Test Section, After-Shock, and Stagnation Conditions in Hotshot Tunnels using Real Nitrogen at Temperatures from 3000 to 4000°K," Arnold Engineering Dev. Center, AEDC-TN-61-82, July 1961.

30. Smith, C. E., Jr., "Thermodynamic Properties of Nitrogen," Lockheed Missiles and Space Co., Rept. 6-90-62-111, Dec. 1962.

31. Heims, Steve P., "Effects of Chemical Dissociation and Moelcular Vibrations on Steady One-Dimensional Flow," NASA TN-D-87, Aug. 1959.

32. French, E. P., des Jardius, P. R., Radbill, J. R., Luntz, N. G., "Computer Programs for Thermodynamic Properties of Air and Homonuclear Diatomic Gases," presented at Supersonic Tunnel Association Meeting, Apr. 1962.

33. Hansen, C. F., "Approximations for the Thermodynamic and Transport Properties of High Temperature Air," NASA TR R-50, 1959.

34. Lee, . . ., "Empirical Relationships between Test Section and Stagnation Chamber Conditions in a High Temperature Wind Tunnel using Air," presented at Supersonic Tunnel Association Meeting, Oct. 1962.

35. Hochstim, A. R., "Approximations to High-Temperature Thermodynamics of Air in Closed Form," Kinetics, Equilibria and Performance of High Temperature Systems, Proc. of the First Conference, Butterworth and Co., Ltd., London, (1960).

36. Bray, K. N. C., "Atomic Recombination in a Hypersonic Wind Tunnel Nozzle," J. Fl. Mech., v. 6, pt. 1, pp. 1-3, July 1959.

37. Hall, J. G., Russo, A. L., "Studies of Chemical Nonequilibrium in Hypersonic Nozzle Flows," Cornell Aero. Lab., Rept. AD-1118-A-6, 1959.

38. Eschenroeder, A. Q., Boyer, D. W., Hall, J. G., "Exact Solutions for Nonequilibrium Expansions of Air with Coupled Chemical Reactions," Cornell Aero. Lab., Rept. AF-1413-A-1, 1961.

39. Bray, K. N. C., Appleton, J. P., "Atomic Recombination in Nozzles: Methods of Analysis for Flows with Complicated Chemistry," Univ. of Southampton, Rept. AASU 166, 1961.

40. Anderson, J. P., "The Effect of Recombination Rate on the Flow of a Dissociating Diatomic Gas," Arnold Engineering Dev. Center, AEDC-TR-61-12, Sept. 1961.

41. Glowacki, W. J., "Effect of Finite Oxygen Recombination Rate on the Flow Conditions in Hypersonic Nozzles," U. S. Naval Ordnance Lab., NOLTR 61-23, 15 Sept. 1961.

42. Bray, K. N. C., "A Simplified Sudden Freezing Analysis for Nonequilibrium Nozzle Flows," Univ. of Southampton, AASU 161, Dec. 1960.

43. Lukasiewicz, J., discussion in, "An Assessment of our Present Status and Further Requirements for High Temperature Hypersonic Facilities, Round Table Discussion," Training Center for Experimental Aerodynamics, Rhode Saint Genese, Belgium, TCEA TM 14, 6 Apr. 1962.

44. Emanuel, G., Vincenti, W. G., "Method for Calculation of the One-Dimensional Nonequilibrium Flow of a General Gas Mixture through a Hypersonic Nozzle," Arnold Engineering Dev. Center, AEDC-TDR-62-131, June 1962.

45. Levinsky, E. S., Brainerd, J. J., "Inviscid and Viscous Hypersonic Nozzle Flow with Finite Rate Chemical Reactions," Arnold Engineering Dev. Center, AEDC-TDR-63-18, Jan. 1963.

46. Sivells, J. C., Payne, R. G., "A Method of Calculating Turbulent Boundary Layer Growth at Hypersonic Mach Numbers," Arnold Engineering Dev. Center, AEDC-TR-59-3, Mar. 1959.

47. Bartz, D. R., "An Approximate Solution of Compressible Turbulent Boundary Layer Development," Trans. ASME, Nov. 1955.

48. Michel, R., "Developpement de la Couche Limite Dans une Tuyere Hypersonique," presented at AGARD Specialists Meeting, High Temperature Aspects of Hypersonic Flow, Rhode Saint Genese, Belgium, Apr. 1962.

49. Reshotko, E., Tucker, M., "Approximate Calculation of the Compressible Turbulent Boundary Layer with Heat Transfer and Arbitrary Pressure Gradient," NACA TN 4154, Dec. 1957.

50. VanDriest, "Turbulent Boundary Layer in Compressible Fluids," J. Aero. Sci., Mar. 1951.

51. Persh, J., Lee, R., "A Method for Calculating Turbulent Boundary Layer Development and Convective Heat Transfer in Convergent-Divergent Nozzles," NAVORD Rept. 4200, June 1956.

52. Burke, A. F., "Turbulent Boundary Layers on Highly Cooled Surfaces at High Mach Numbers," ASD Symposium on Aeroelasticity, Wright-Patterson Air Force Base, Ohio, Oct. 30-Nov. 1, 1961.

53. Lee, J., "Axisymmetric Nozzles for Hypersonic Flow," Ohio State Research Foundation, Rept. 459-1, July 1959.

54. Schlichting, H., "Berechnung der Strömung in rotationsymmetrischen Diffusoren mit Hilfe der Grenzschicht-theorie," z. Flugwissenschaften, v. 9, n. 4/5, (1961).

55. Goldstein, S., ed., Modern Developments in Fluid Dynamics, v. 1, Clarendon Press, Oxford, p. 304, 1938.

56. Durand, J. A., Potter, J. L., "Calculation of Thicknesses of Laminar Boundary Layers in Axisymmetric Nozzles with Low Density, Hypervelocity Flows," Arnold Engineering Dev. Center, AEDC-TN-61-146, Dec. 1961.

57. Shapiro, A. H., The Dynamics and Thermodynamics of Compressible Fluid Flow, Vol. II, Ronald Press, New York, 1954.

58. Schlichting, H., Boundary Layer Theory, McGraw Hill, New York, 1955.

59. Dorrance, W. H., Viscous Hypersonic Flow, McGraw Hill, New York, 196[illegible]

60. Lees, L., "Laminar Heat Transfer over Blunt-Nosed Bodies at Hypersonic Flight Speeds," Jet Propulsion, v. 36, pp. 259-269 (1956).

61. Schubauer, G. B., Tchen, C. M., "Turbulent Flow," Section B, "Turbulent Flows and Heat Transfer," v. V of Princeton Series, High Speed Aerodynamics and Jet Propulsion, C. C. Lin, ed., Princeton Univ. Press, 1959.

62. Shapiro, A. H., The Dynamics and Thermodynamics of Compressible Fluid Flow, v. II, Chapt. 27, Ronald Press, 1954.

63. Cohen, N. B., "A Method for Computing Turbulent Heat Transfer in the Presence of a Streamwise Pressure Gradient for Bodies in High Speed Flow," NASA Memo 1-2-59L, Mar. 1959.

64. Spence, D. A., "Distributions of Velocity, Enthalpy and Shear Stress in the Compressible Turbulent Boundary Layer on a Flat Plate," Royal Aircraft Establishment (Farnborough), Rept. AERO 2631, Nov. 1959.

65. Persh, J., "A Theoretical Investigation of Turbulent Boundary Layer Flow with Heat Transfer at Supersonic and Hypersonic Speeds," NAVORD Rept. 3854, May 1955.

66. Eckert, E. R. G., "Engineering Relations for Heat Transfer and Friction in High-Velocity Laminar and Turbulent Boundary Layer Flow over Surfaces with Constant Pressure and Temperature," Trans. ASME, v. 78, no. 6, p. 1273, Aug. 1956.

67. Rose, P. H., Probstein, R. F., and Adams, M. C., "Turbulent Heat Transfer Through a Highly Cooled Partially Dissociated Boundary Layer," JAS, v. 25, pp. 751-760, Dec. 1958.

68. Matting, J. W., Chapman, D. R., Nyholm, J. R., and Thomas, A. G., "Turbulent Skin Friction at High Mach Numbers and Reynolds Numbers in Air and Helium," NASA TR R-82, 1961.

69. Hidalgo, H., "On the Application of VanDriest's Method to a Highly Cooled, Partially Dissociated Turbulent Boundary Layer," Jet Propulsion, v. 28, no. 7, pp. 487-489, July 1958.

70. Reece, J. W., "Test Section Conditions Generated in the Supersonic Expansion of Real Air," JAS, v. 29, pp. 617-618, May 1962.

71. Hilsenrath, J., and Beckett, C. W., "Tables of Thermodynamic Properties of Argon-Free Air to 15,000°K," Arnold Engineering Dev. Center, AEDC-TN-56-12, Sept. 1956.

72. Lukasiewicz, J., Jackson, R., Whitfield, J. D., "Status of Development of Hotshot Tunnels at the AEDC," paper presented at AGARD Meeting on High Temperature Aspects of Hypersonic Flow, Rhode-Saint-Genese, Belgium, Apr. 3-6, 1962.

73. Sherman, P. M., Early, H. C., Lawrence, W. N., "Design Considerations for Arc Heated Hypersonic Tunnel," Final Rept., ORA Project 02953, The Univ. of Mich., July 1960.

74. Whitfield, J. D., Private Communication, Arnold Engineering Development Center, AEDC, Tullahoma, Tenn., 1961.

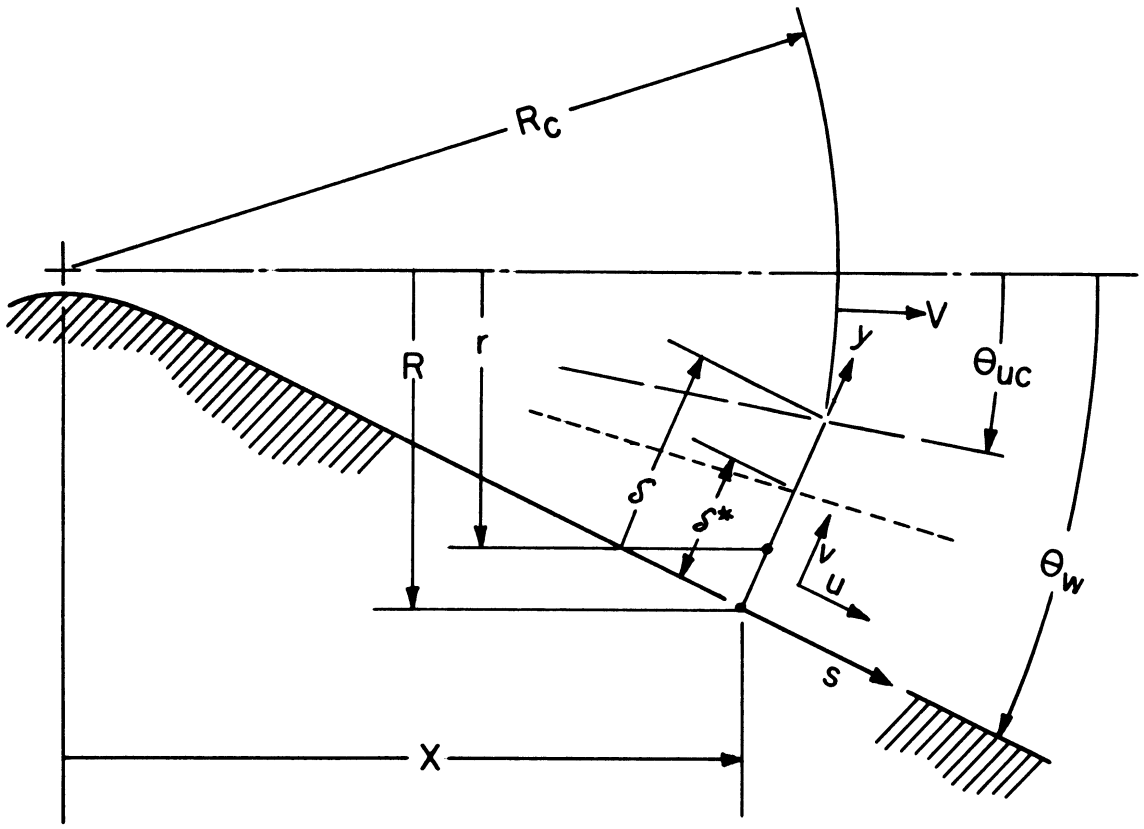

FIGURE I. CONICAL NOZZLE BOUNDARY LAYER CO-ORDINATE SYSTEM.

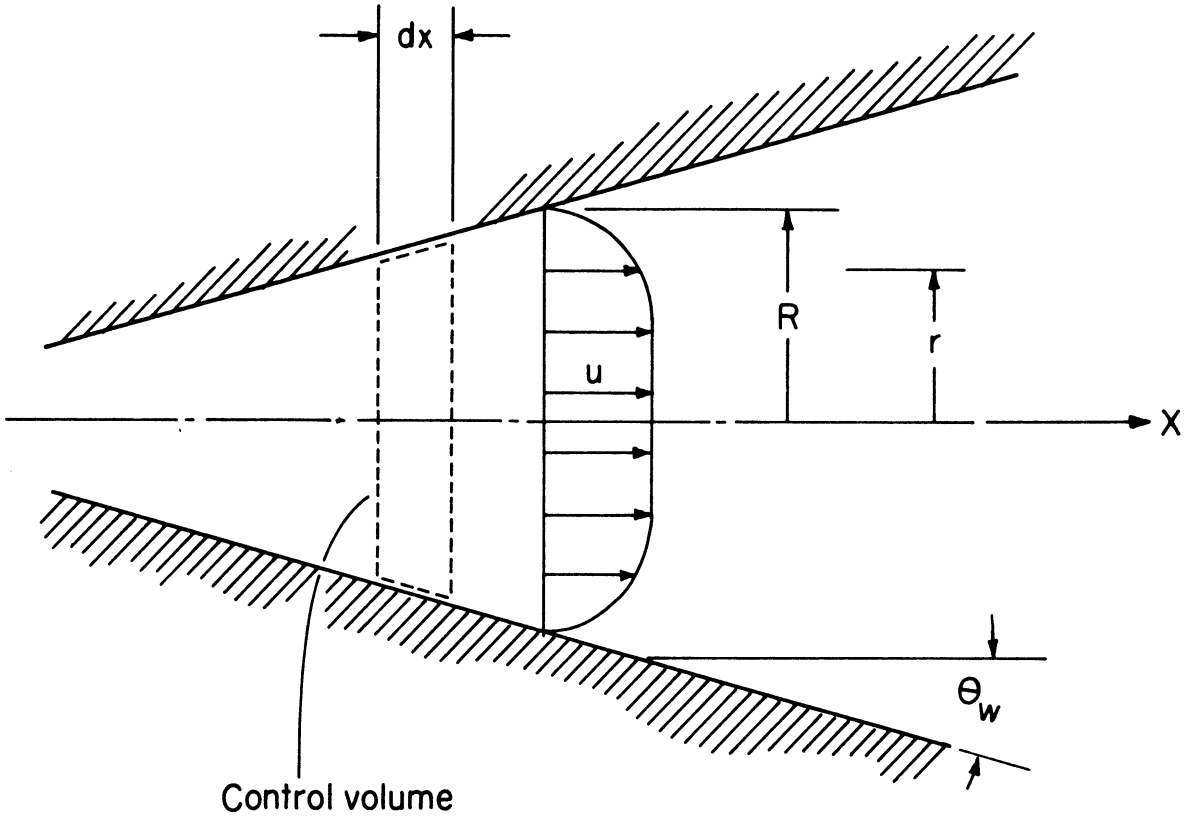

FIGURE 2. APPROXIMATE NOZZLE VELOCITY DISTRIBUTION FOR THE CASE $\theta_w \ll 1$.

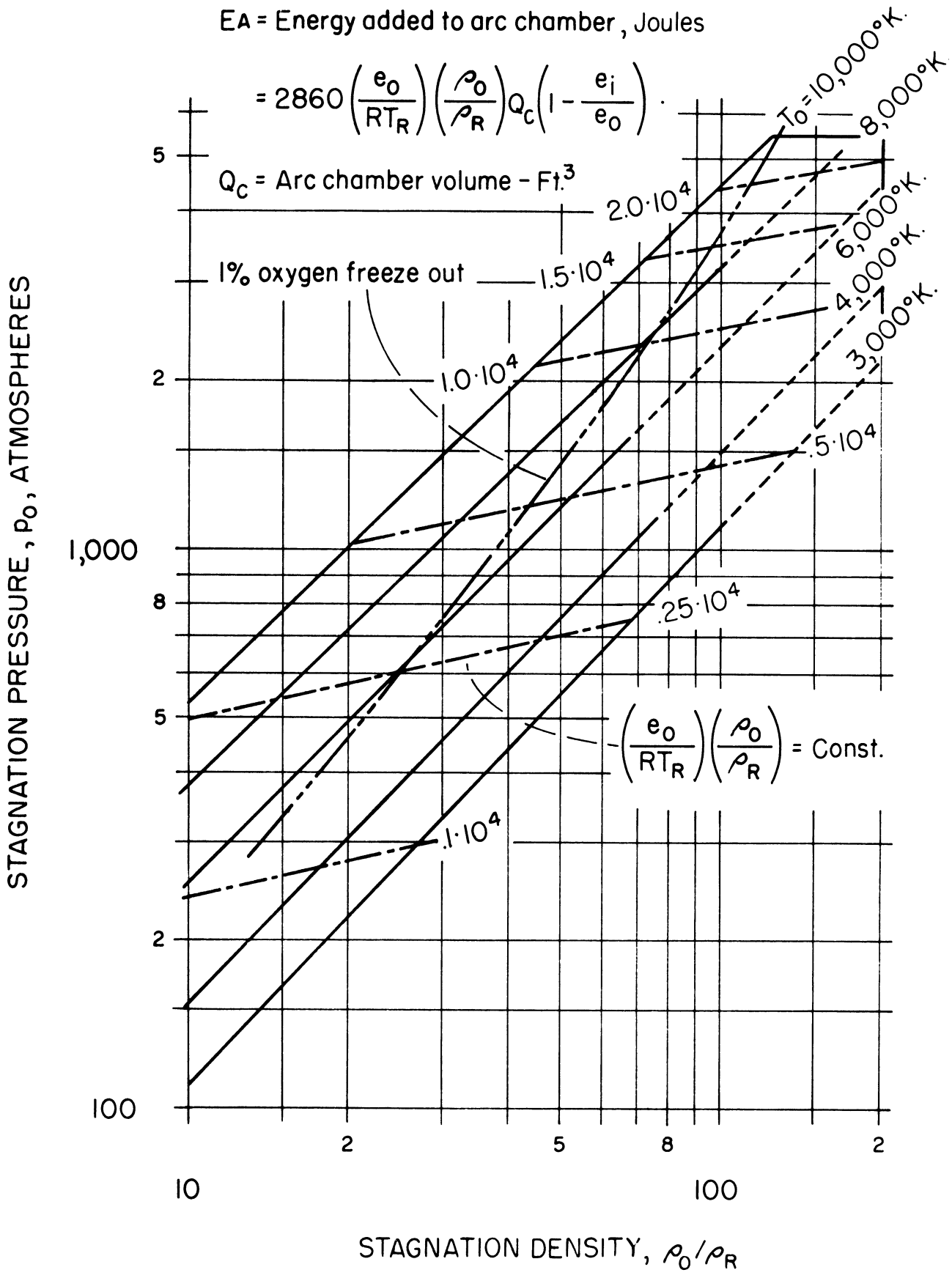

FIGURE 3. ARC CHAMBER CONDITIONS FOR EQUILIBRIUM AIR (Thermodynamic data from Ref. 20).

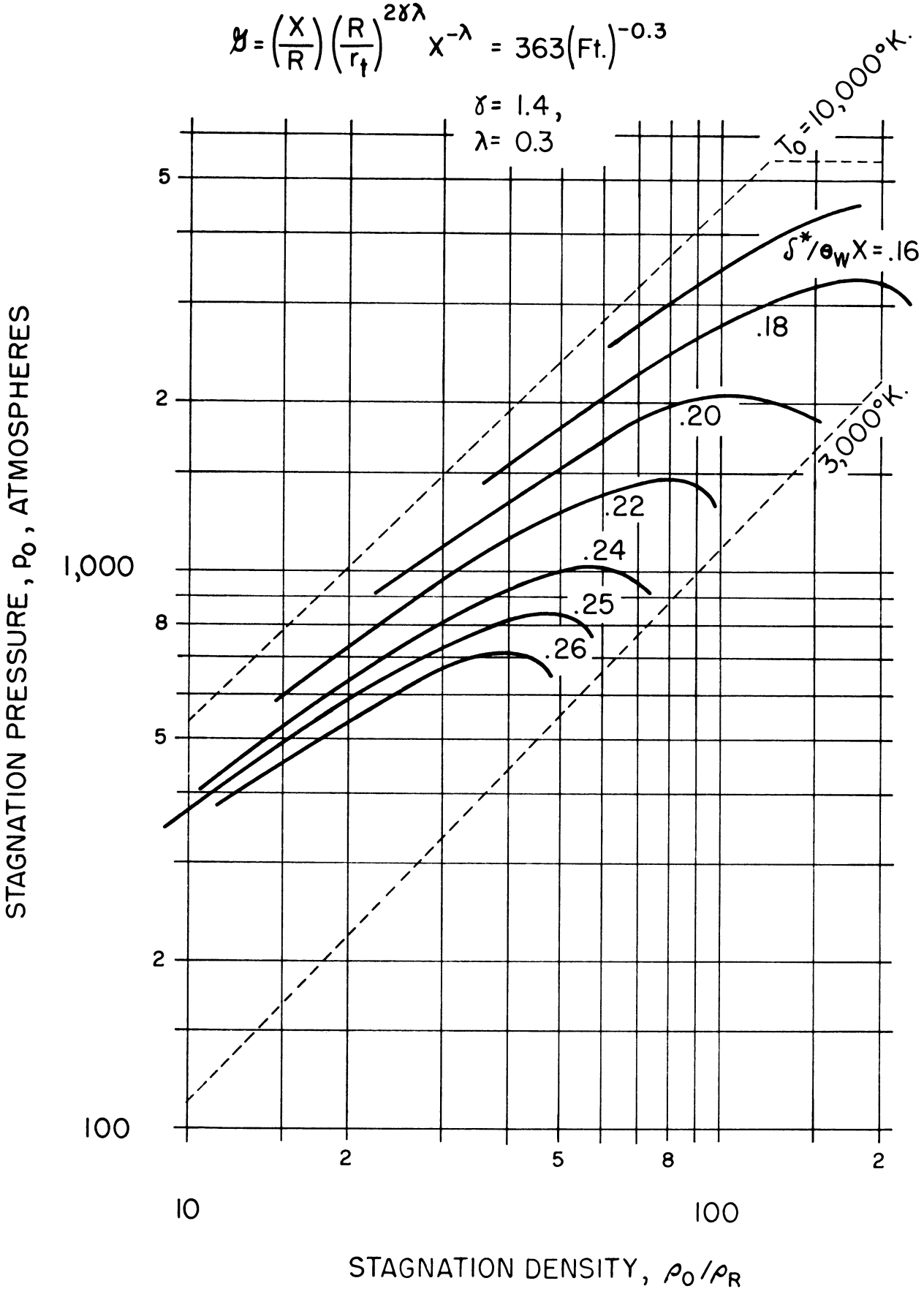

FIGURE 4. VARIATION OF TEST SECTION BOUNDARY LAYER THICKNESS WITH STAGNATION CONDITIONS.

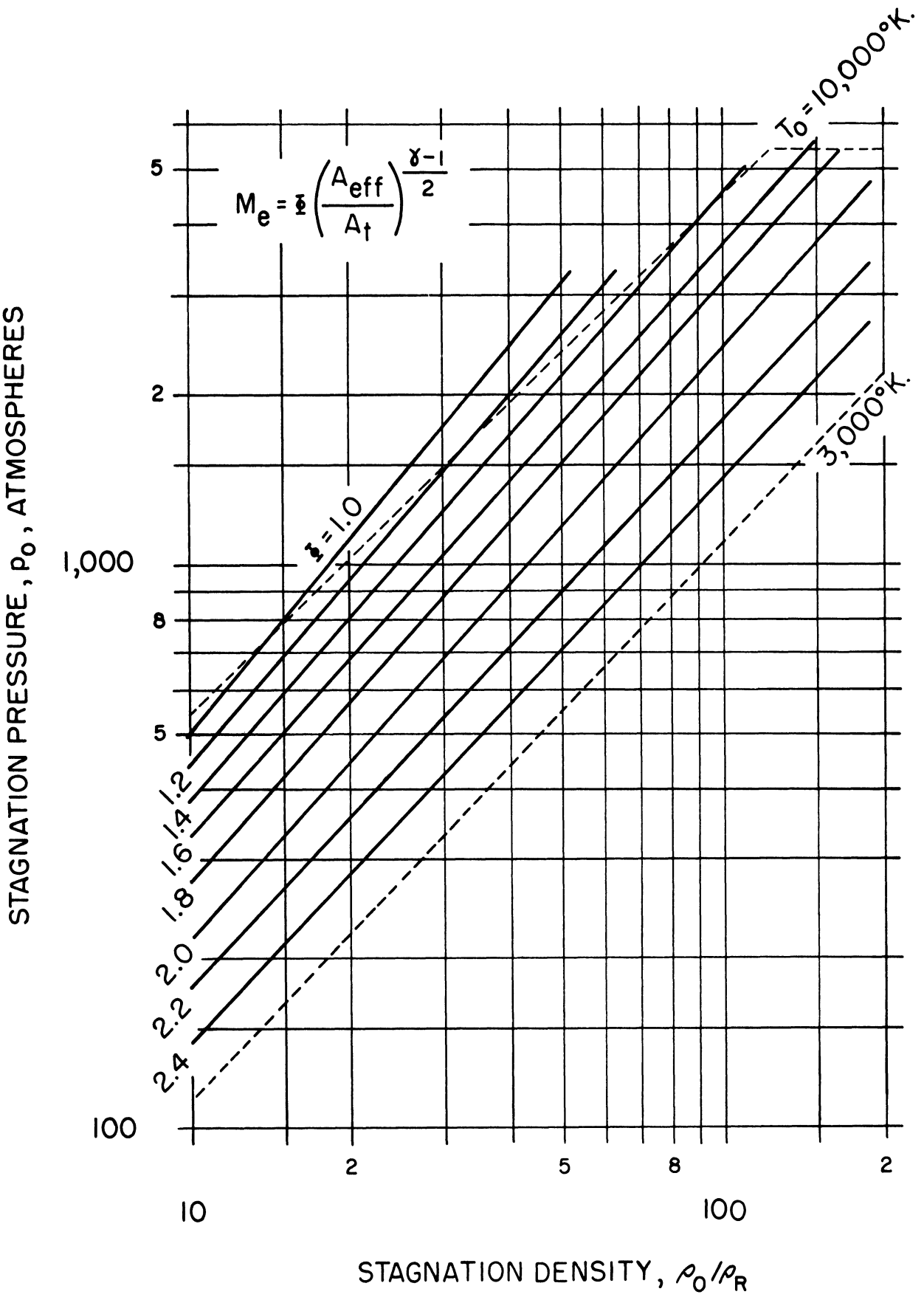

FIGURE 5. THE MACH NUMBER FUNCTION $\mathfrak{F}$ FOR EQUILIBRIUM AIR.

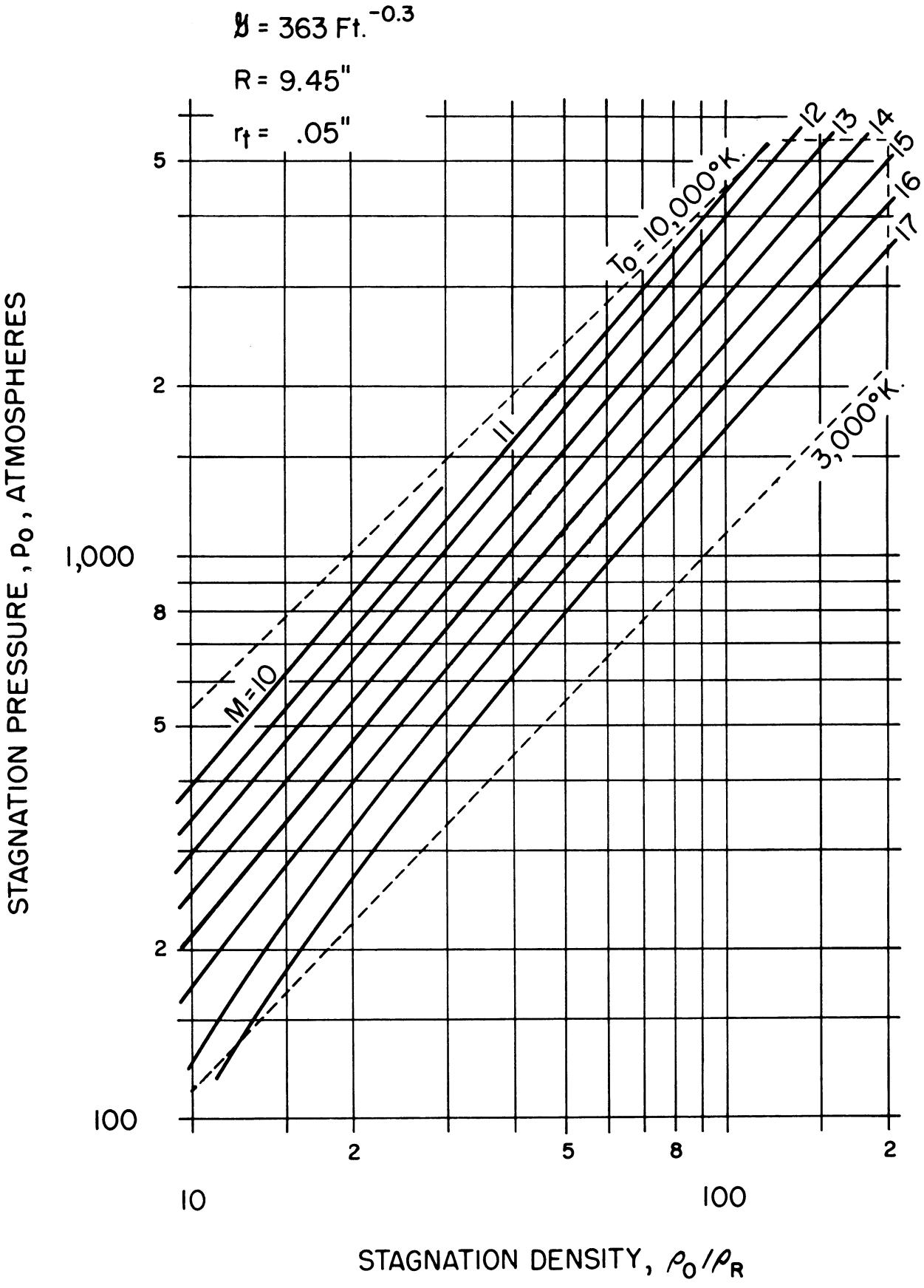

FIGURE 6. VARIATION OF TEST SECTION MACH NUMBER WITH STAGNATION CONDITIONS.

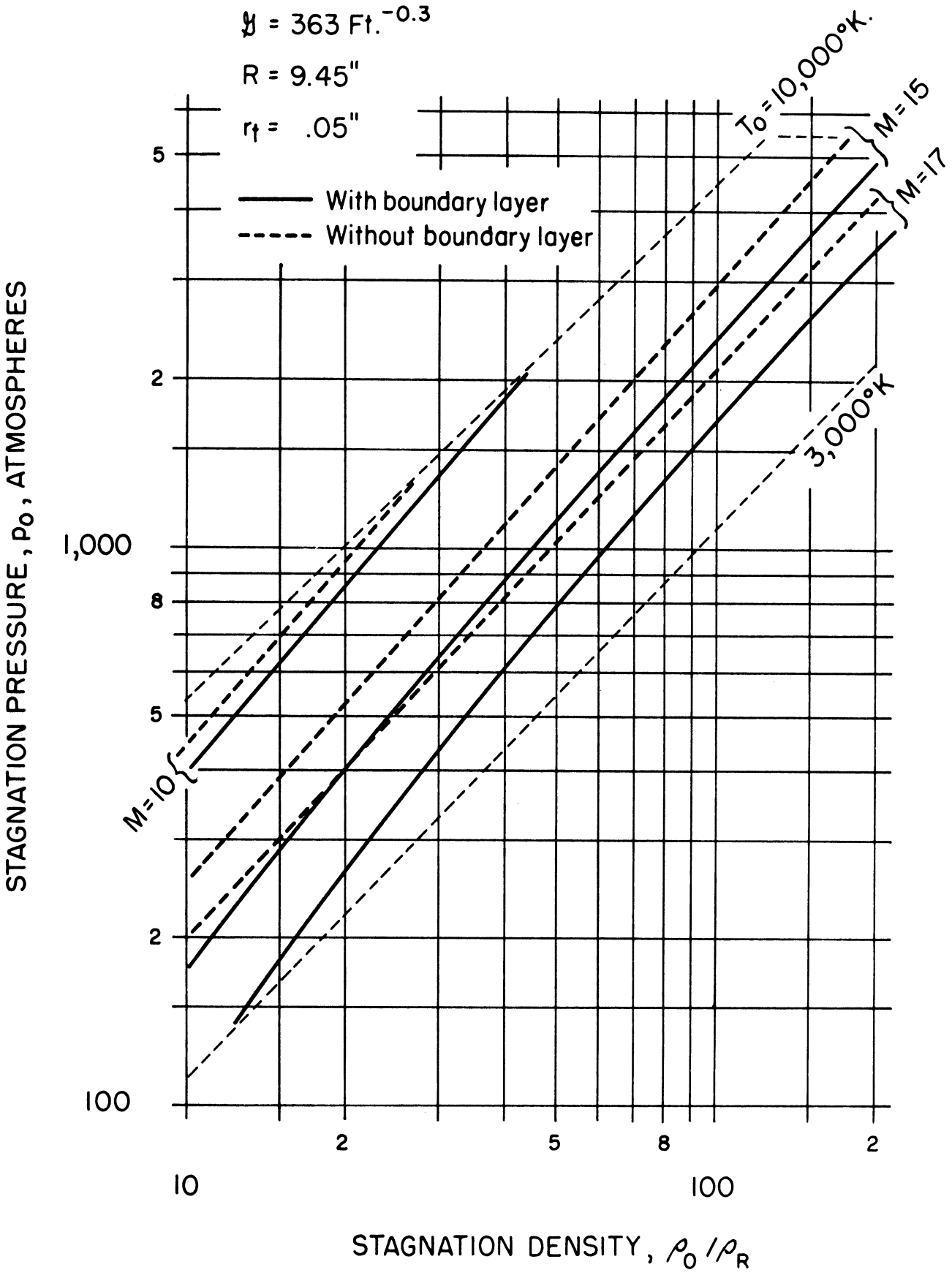

FIGURE 7. THE EFFECT OF THE BOUNDARY LAYER UPON THE TEST SECTION MACH NUMBER.

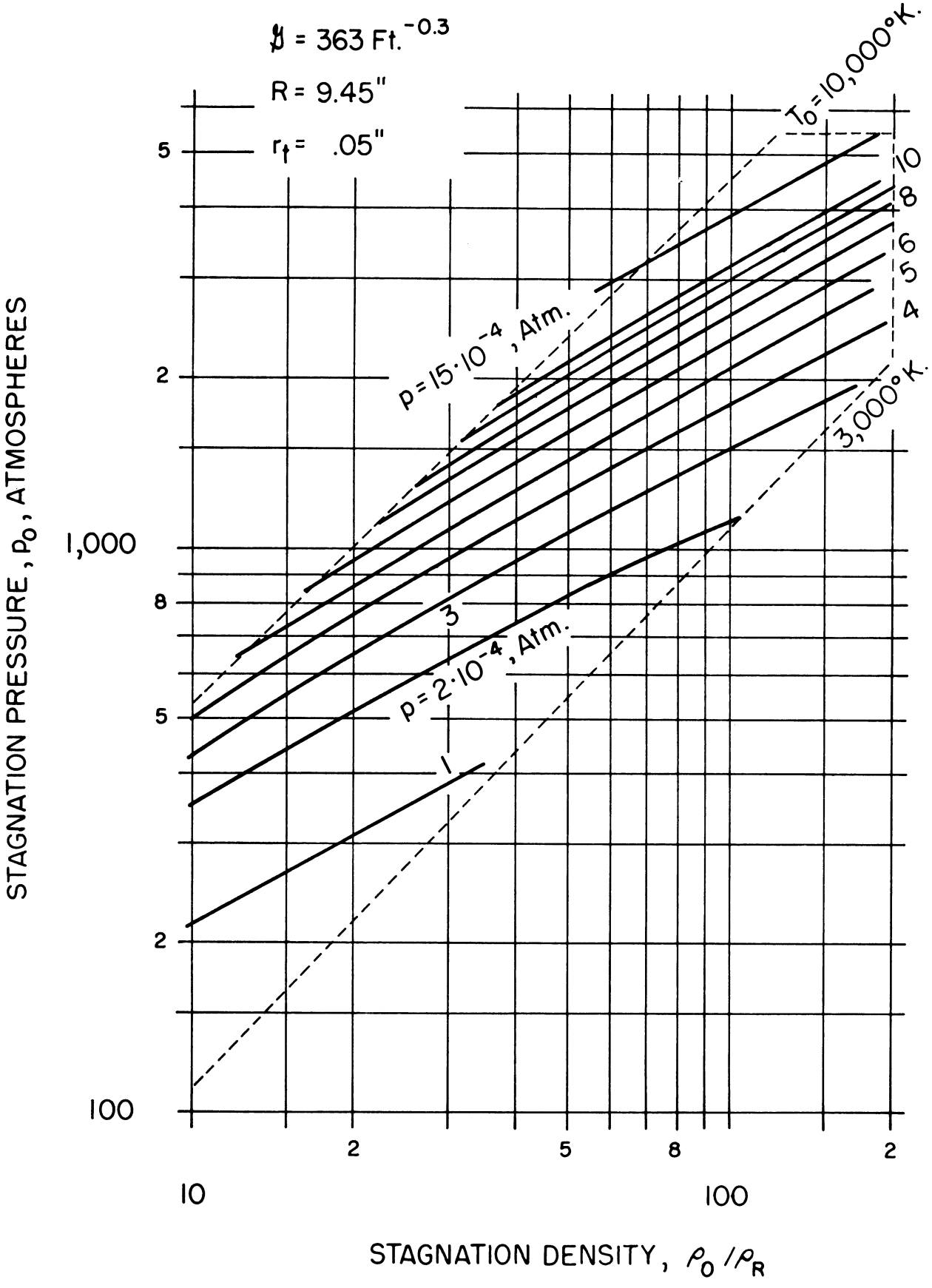

FIGURE 8. VARIATION OF TEST SECTION STATIC PRESSURE WITH STAGNATION CONDITIONS.

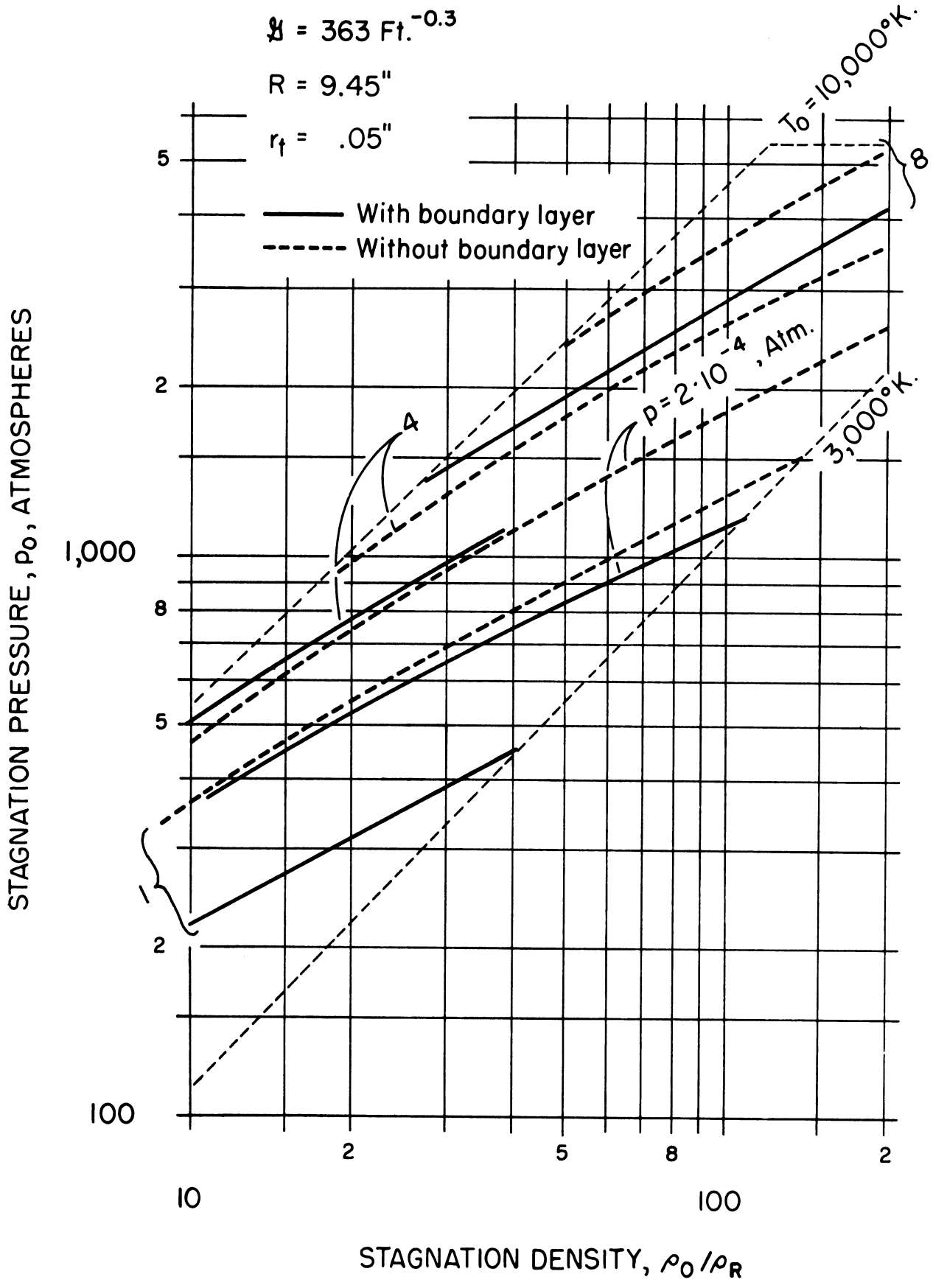

FIGURE 9. THE EFFECT OF THE BOUNDARY LAYER UPON THE TEST SECTION STATIC PRESSURE.

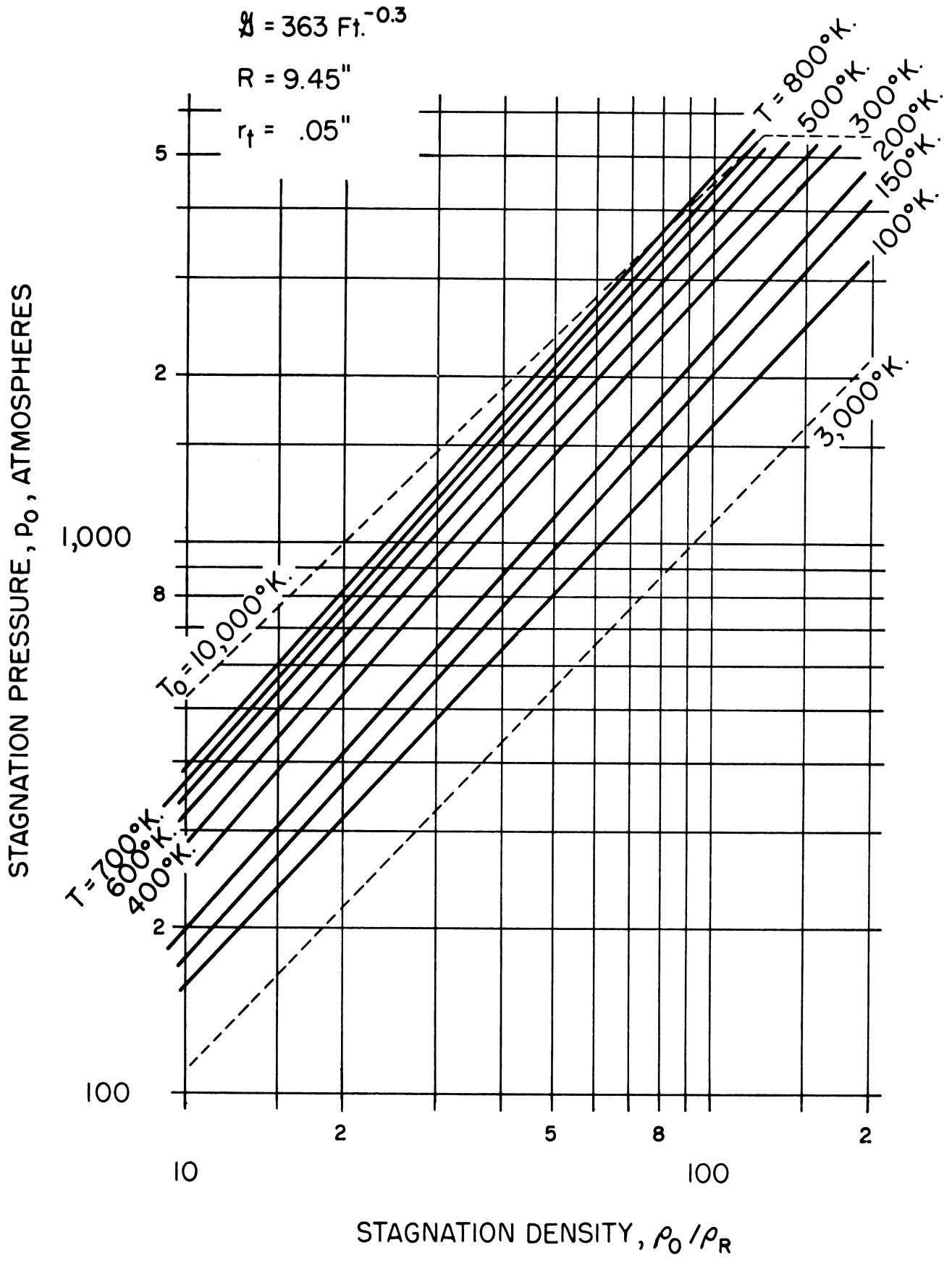

FIGURE 10. VARIATION OF TEST SECTION STATIC TEMPERATURE WITH STAGNATION CONDITIONS.

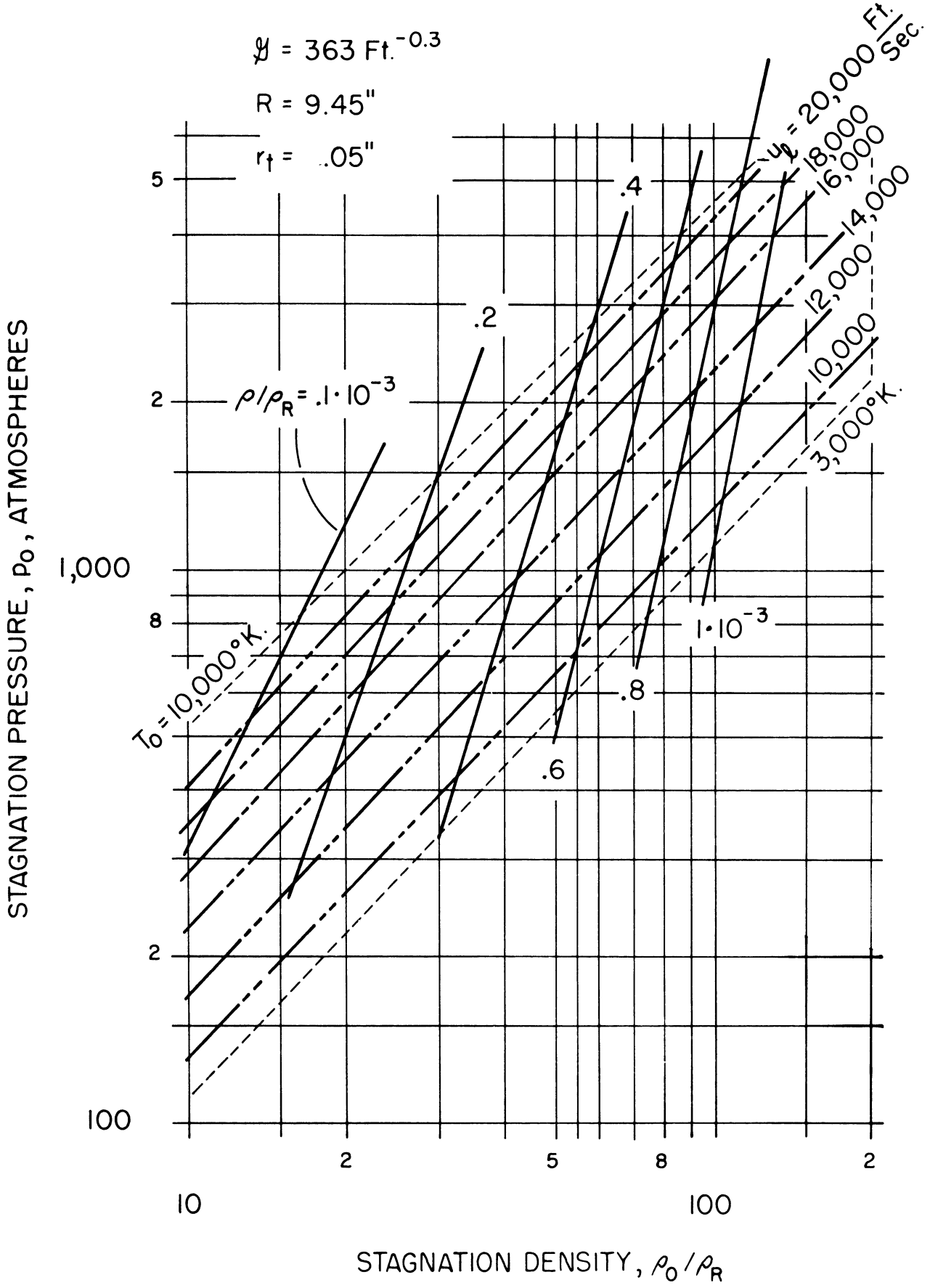

FIGURE 11. VARIATION OF TEST SECTION DENSITY AND LIMITING VELOCITY WITH STAGNATION CONDITIONS.

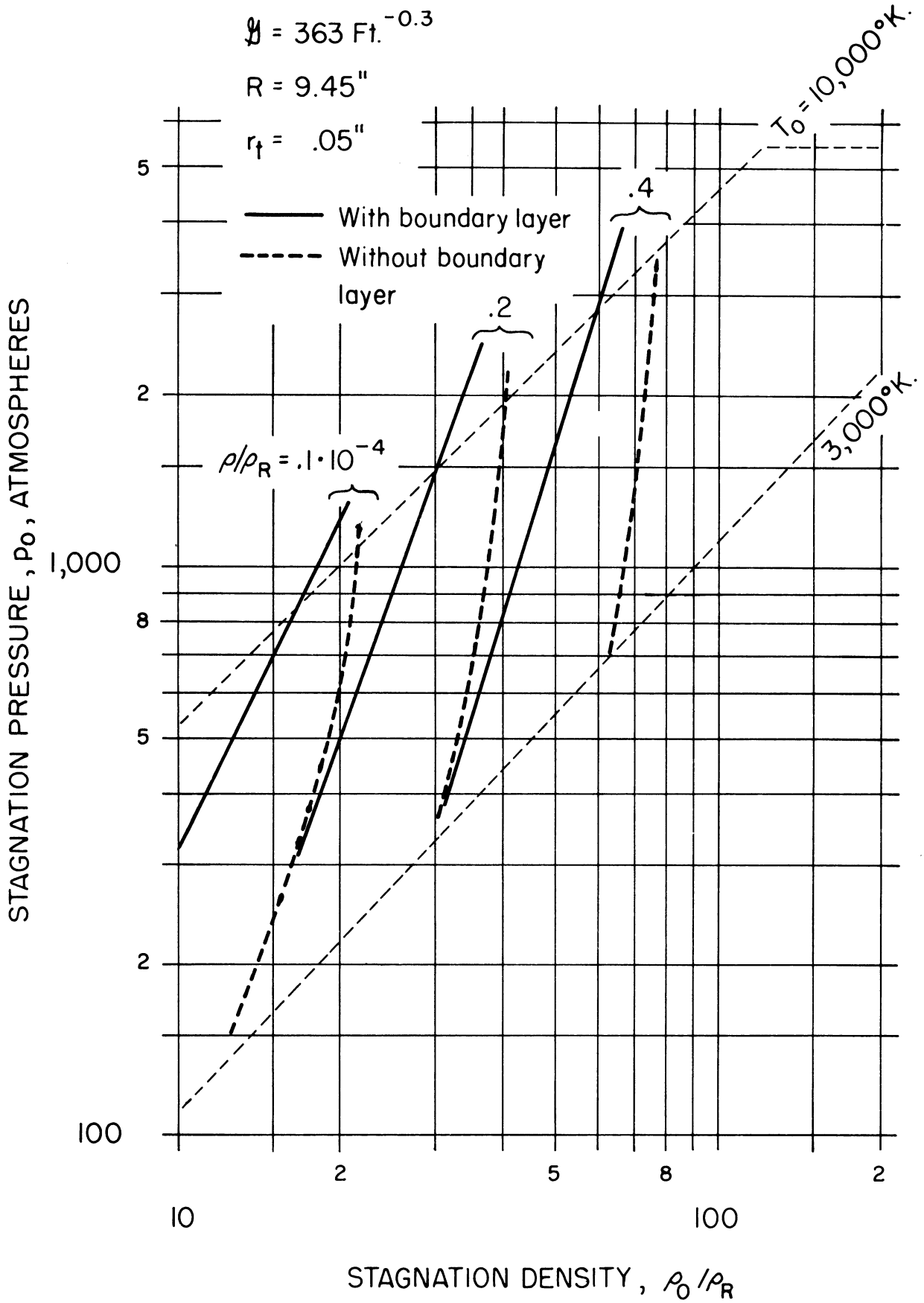

FIGURE 12. THE EFFECT OF THE BOUNDARY LAYER UPON THE TEST SECTION DENSITY.

APPENDIX A

It has been shown that the mass flow through the nozzle is

$$\dot{m} = 2\pi \rho_e V_e \left[R_c^2 (1 - \cos \theta_{uc}) + \left(R\delta - \frac{\delta^2}{2} \cos \theta_w \right) \cos (\theta_w - \theta_{uc}) \right.$$

$$\left. - \left(R\delta^* - \frac{\delta^{*2}}{2} \cos \theta_w \right) \cos (\theta_w - \theta_{uc}) \right] \quad . \tag{A-1}$$

Now let

$$\alpha = \theta_w - \theta_{uc} \tag{A-2}$$

then from Figure 1 it can be seen that

$$R_c = \frac{R}{\cos \alpha \sin \theta_w}$$

$$\delta = R_c \sin \alpha = R \frac{\tan \alpha}{\sin \theta_w} \quad . \tag{A-3}$$

It follows that

$$\frac{m}{2\pi \rho_e V_e} = \frac{R^2 (1 - \cos \theta_{uc})}{\cos^2 \alpha \sin^2 \theta_w} + \cos \alpha \left[R^2 \frac{\tan \alpha}{\sin \theta_w} - \frac{1}{2} R^2 \frac{\tan^2 \alpha \cos \theta_w}{\sin^2 \theta_w} \right]$$

$$- \cos \alpha \left(R\delta^* - \frac{\delta^{*2}}{2} \cos \theta_w \right) \tag{A-4}$$

Now assuming that

$$\theta_w, \ \theta_{uc}, \ \alpha << 1 \tag{A-5}$$

series expansion of the trigonometric functions yields the following for the terms in Equation A-4:

$$\frac{R^2 (1 - \cos \theta_{uc})}{\cos^2 \alpha \sin^2 \theta_w} = \frac{R^2}{2} \left(1 - \frac{2\alpha}{\theta_w} + \frac{\alpha^2}{\theta_w^2}\right) \left(1 + \frac{\theta_w^2}{4} + \frac{11\alpha^2}{12} + \frac{\theta_w \alpha}{6}\right) \quad , \tag{A-6}$$

$$\cos \alpha \left[\frac{R^2 \tan \alpha}{\sin \theta_w} - \frac{1}{2} R^2 \frac{\tan^2 \alpha \cos \theta_w}{\sin^2 \theta_w}\right] =$$

$$R^2 \left[\frac{\alpha}{\theta_w} \left(1 - \frac{\alpha^2}{6} + \frac{\theta_w^2}{6}\right) - \frac{1}{2} \frac{\alpha^2}{\theta_w^2} \left(1 + \frac{\alpha^2}{6} - \frac{\theta_w^2}{6}\right)\right] \quad , \tag{A-7}$$

$$\left(R\delta^* - \frac{\delta^{*2}}{2} \cos \theta_w\right) \cos \alpha = R\delta^* \left(1 - \frac{\alpha^2}{2}\right) - \frac{\delta^{*2}}{2} \left(1 - \frac{\theta_w^2}{2} - \frac{\alpha^2}{2}\right) \quad . \tag{A-8}$$

Combining these results, introducing a new parameter σ defined as

$$\sigma = \frac{\delta}{\delta^*}$$

and using the relations

$$\frac{\delta}{R} = \sigma \frac{\delta^*}{R} = \frac{\tan \alpha}{\sin \theta_w} \simeq \frac{\alpha}{\theta_w} + O(\theta_w^2)$$

Equation A-4 can be written in the form

$$\frac{\dot{m}}{\pi \rho_e V_e} = (R - \delta^*)^2 \left[1 + \theta_w^2 E(\sigma, \frac{\delta^*}{R}) + O(\theta_w^4)\right] \quad ,$$

where the function E is given by

$$E(\sigma, \frac{\delta^*}{R}) = \frac{\frac{1}{4} + \left(1 - \frac{1}{2\sigma^2}\right) \left(\sigma \frac{\delta^*}{R}\right)^2 - (2 - \frac{1}{\sigma}) (\sigma \frac{\delta^*}{R})^3 + \left(\frac{3}{4} - \frac{1}{2\sigma^2}\right) \sigma \frac{\delta^*}{R}^4}{\left(1 - \frac{\delta^*}{R}\right)^2}$$

The function $E(\sigma; \frac{\delta^*}{R})$ is plotted in Figure A-1 for $\sigma = 1.0$ and 2.0.

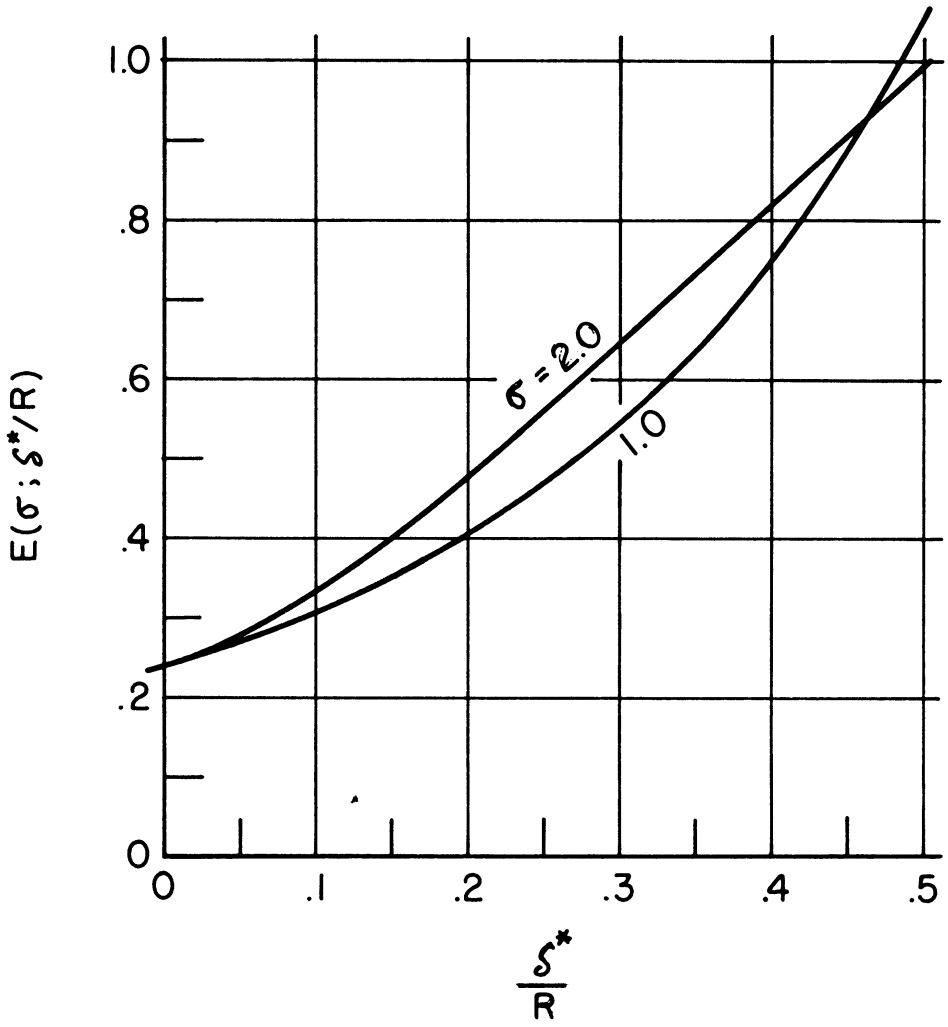

FIGURE A-1. MASS FLOW CORRECTION FACTOR $E\left(\sigma; \frac{\delta^*}{R}\right)$.

APPENDIX B

In order to estimate the effect of transverse curvature upon the skin friction coefficient in incompressible flow consider the case of an axisymmetric boundary layer with R and u_e constant, even though this case is not entirely realistic from a physical point of view. The momentum equation becomes

$$\frac{d\overline{\delta_2}}{dx} = \frac{c_f}{2} \tag{B-1}$$

Now c_f is assumed to be given by the power law (Equation 30)

$$c_f = A\left(\frac{\rho_e u_e \delta}{\mu_e}\right)^{-m} \tag{30}$$

and correspondingly the velocity distribution will be

$$\left(\frac{u}{u_e}\right) = \left(\frac{y}{\delta}\right)^s \tag{B-2}$$

where $s = \frac{m}{2 - m}$. From Equations 9 and 12 it now follows that

$$\overline{\delta_2} = \delta \int_0^1 \left[1 - \frac{\delta}{R}\left(\frac{y}{\delta}\right)\right]\left(\frac{y}{\delta}\right)^s \left[1 - \left(\frac{y}{\delta}\right)^s\right] d\left(\frac{y}{\delta}\right) \tag{B-3}$$

so that

$$\overline{\delta_2} = \delta\left(k_1 - k_2 \frac{\delta}{R}\right) \tag{B-4}$$

where

$$k_1 = \frac{1}{s+1} - \frac{1}{2s+1} \quad ; \qquad k_2 = \frac{1}{s+2} - \frac{1}{2s+2} \quad .$$

Combining Equations 30, B-1, and B-4 yields the following differential equation for the boundary layer thickness δ:

$$\frac{d\delta}{dx} = \frac{\frac{A}{2}\left(\frac{\rho_e u_e \delta}{\mu_e}\right)^{-m}}{\left(k_1 - 2k_2 \frac{\delta}{R}\right)} \tag{B-5}$$

Equation B-5 shows that the rate of boundary layer growth increases with increasing δ/R. Thus one reaches the tentative conclusion that in internal flows the transverse curvature results in thicker boundary layers than in the cases in which the transverse curvature effect is absent. Integrating Equation B-5 and assuming that $\delta = 0$ when $x = 0$ yields the result

$$Re_\delta^{m+1}\left(\frac{k_1}{m+1}\right)\left[1 - \frac{2k_2}{k_1}\left(\frac{m+1}{m+2}\right)\frac{\delta}{R}\right] = \frac{A}{2} Re_x \quad . \tag{B-6}$$

It must be pointed out that the assumption $\delta = 0$ when $x = 0$ is inconsistent with the fact that $\delta/R \sim O(1)$ and the assumption that u_e and R are constant. Nevertheless the results of the integration above may be valid in the limiting case when δ/R is quite small.

In the absence of transverse curvature ($\delta/R = 0$) Equation B-6 together with Equation 30 immediately leads to flat plate power law for the friction coefficient (Equation 32). Clearly as $\delta/R \sim O(1)$, c_f can no longer be expressed as a simple power of Re_x, rather

$$c_f = \left[\frac{\frac{A}{2} Re_x}{1 - \frac{2k_2}{k_1}\left(\frac{m+1}{m+2}\right)\frac{\delta}{R}}\left(\frac{m+1}{k_1}\right)\right]^{-\frac{m}{m+1}} \tag{B-7}$$

and from Equation B-7 it follows that the transverse curvature effect decreases the skin friction coefficient.

If δ/R is sufficiently small it can be shown from Equation B-6 that to first order in δ/R

$$\delta = \delta_P \left[1 + \frac{2k_2}{k_1 (m + 2)} \frac{\delta_P}{R} \right] \tag{B-8}$$

where δ_P is the plane value of boundary layer thickness given by

$$\delta_P = x \left(\frac{u_e x}{\nu_e} \right)^{-\frac{m}{m+1}} \left(\frac{m + 1}{k_1} \frac{A}{2} \right)^{\frac{1}{m+1}} . \tag{B-9}$$

From Equations 30, B-8, and B-9 it follows that to first order in δ/R

$$c_f = c_{f_P} \left[1 - k_4 \frac{x}{R} (Re_x)^{-\frac{m}{m+1}} \right] \tag{B-10}$$

where

$$k_4 = \frac{2mk_2}{k_1 (m + 2)} \left(\frac{m + 1}{k_1} \frac{A}{2} \right)^{\frac{1}{m+1}} .$$

APPENDIX C

Burke[3] used the empirical displacement thickness relation either of the form

$$\frac{\delta^*}{x} = .0463 \frac{M_e^{1.311}}{Re_x^{0.276}} \tag{C-1}$$

or of the form

$$\frac{\delta^*}{x} = 0.49 \left(\frac{\rho^* u_e x}{\mu^*} \right)^{-0.3} \tag{C-2}$$

in conjunction with the continuity equation

$$\dot{m} = \pi \rho_e u_e (R - \delta^*)^2 \tag{7}$$

to calculate the combined nozzle and boundary layer flow at the test section. At the hypersonic test section conditions of interest the static temperature of the isentropic core is low so that the perfect gas assumption is applicable. In this case, Reece[70] has shown that the usual perfect gas nozzle flow equations can be used with correction factors to account for the real gas effects in the reservoir and upstream portion of the nozzle. Consequently static temperature and pressure are determined from the equations

$$\frac{h_o}{h} = 1 + \frac{\gamma - 1}{2} M_e^2 \quad , \tag{C-3}$$

$$T = \frac{h}{\frac{\gamma}{\gamma - 1} R}$$

and

$$\frac{p}{p_o} = \left(1 + \frac{\gamma - 1}{2} M^2 \right)^{-\frac{\gamma}{\gamma - 1}} e^{-\frac{\Delta S}{R}} \quad . \tag{C-4}$$

The ratio of nozzle to throat area is written in the form

$$\frac{A}{A_t} = f_1 (h_o, p_o) \left(\frac{\gamma + 1}{2}\right)^{-\frac{\gamma + 1}{2(\gamma - 1)}} M_e^{-1} \left(1 + \frac{\gamma - 1}{2} M_e^2\right)^{\frac{\gamma + 1}{2(\gamma - 1)}} , \qquad \text{(C-5)}$$

and the mass flow density at the nozzle throat is related to reservoir conditions by

$$\frac{\sqrt{h_o}}{p_o} \rho_t a_t = f_2 (h_o, p_o)\, G_1 \qquad \text{(C-6)}$$

$$G_1 = \sqrt{2} \left(\frac{2}{\gamma + 1}\right)^{\frac{1}{\gamma - 1}} \left(\frac{\gamma}{\gamma - 1}\right) \left(\frac{\gamma - 1}{\gamma + 1}\right)^{\frac{1}{2}}$$

Equations C-1 to C-6 form the basis of Burke's calculation method. Before applying these equations it is necessary to discuss the various real gas correction factors.

In Equation C-4

$$\frac{\Delta S}{R} = \frac{S (p_o, h_o)}{R} - \left(\frac{S}{R}\right)_{ideal}$$

where $S(p_o, h_o)/R$ is the real gas dimensionless entropy at stagnation conditions, which in the present case was determined from Feldman's Mollier diagram for argon free air.[20] $(S/R)_{ideal}$ in the perfect gas dimensionless entropy corresponding to h_o and p_o, and given by

$$\left(\frac{S}{R}\right)_{ideal} = \frac{\gamma}{\gamma - 1} \ln \left(\frac{h_o}{h_R}\right) - \ln p_o + \frac{S_R}{R} \quad . \qquad \text{(C-7)}$$

Subscript R refers to the reference condition of 273.16°K and 1 atm pressure. h_R and S_R/R were taken from NBS Circular 564. Since the NBS tables are based on air including argon it has been assumed that h and S/R are the same for real and argon free air at the reference condition. The values of the gas constant R and the molecular weight used here correspond to those given in Reference 20.

The correction factor $f_1 (h_o, p_o)$ in Equation C-5 has been determined from Goin's tables[15] and from graphical calculations using Mollier charts for air.[20] The two calculations were in excellent agreement and the resulting curves for $f_1 (h_o, p_o)$ are shown in Figure C-1. It should be noted that Burke and Reece[3,70] assumed that $f_1 = f_1 (h_o)$ and this is approximately true over the enthalpy range $25 \leq h_o/RT_o \leq 150$ covered by their calculations. At higher values of stagnation enthalpy h_o Figure C-1 shows that f_1 strongly depends upon the stagnation pressure p_o.

The correction factor $f_2 (h_o, p_o)$ in Equation C-6 has been computed using Goin's tables[15] and is plotted in Figure C-2. Once again there are considerable variations in $f_2 (h_o, p_o)$ with p_o at the higher values of stagnation enthalpy.

In using the reference temperature form of the boundary layer correlation (Equation C-2) it becomes necessary to determine the reference temperature T^* from the reference enthalpy h^* as defined by Equation 36. For this purpose an average specific heat, $\overline{C}_P$, defined by

$$\overline{C}_P T^* = h^* = \frac{\gamma R}{\gamma - 1} f_3 (p, h^*) T^* \tag{C-8}$$

has been introduced. To compute this function it has been found convenient to use Blackwell's tables.[14] The function $f_3 (p, h^*)$ is plotted as a function of h^*/RT_R in Figure C-3.

Using the assumption that $\frac{\gamma - 1}{2} M_e^2 >> 1$, letting $h^* \cong 0.235\, h_o$, assuming that the thickness of the boundary layer at the nozzle throat is negligible, and that

$$\mu^* = k_2 (T^*)^{1/2}$$

Burke has shown that Equations C-2 and 7 can be reduced to the single equation

$$\frac{\delta^*}{\theta_w x} = k_5 \zeta \left(1 - \frac{\delta^*}{\theta_w x}\right)^{2\gamma\lambda} \tag{C-9}$$

where for $\lambda = 0.3$, $\gamma = 1.4$,

$$\zeta = \left[\frac{1}{\theta_w} f_1^{-0.12} f_2^{-0.3} \left(\frac{h_o}{p_o}\right)^{0.3}\right]\left[\left(\frac{\theta_w}{r_t}\right)^{0.3} \left(\frac{x\theta_w}{r_t}\right)^{0.54} f_3^{-0.45}\right] ,$$

and for a boundary layer correlation of the form

$$\frac{\delta^*}{x} = k_1 \left(\frac{\rho^* u_e x}{\mu^*}\right)^{-\lambda}$$

the constant k_5 is given by

$$k_5 = k_1 \left\{\frac{\frac{2}{\gamma} G_1 \left(\frac{\gamma R}{\gamma - 1}\right)^{3/2}}{k_2 R(0.22)^{3/2}}\right\}^{-\lambda} \left\{\left(\frac{\gamma - 1}{\gamma + 1}\right)^{\frac{\gamma + 1}{2(\gamma - 1)}}\right\}^{-\lambda(\gamma - 1)} .$$

For the correlation formula (Equation C-2), with $\gamma = 1.4$, $R = 1.724 \times 10^3$ $ft^2/sec^2\ {}^oR$ (argon free air), and $k_2 = 2.01 \times 10^{-8}$ slugs/ft sec ${}^oR^{1/2}$ (taken from Burke[3]) the constant k_5 has the value 0.362×10^{-3} $(ft^2/slug)^{0.3}$.

ζ can be calculated once the stagnation conditions, and the nozzle throat radius, length, and half angle are known. This in turn makes it possible to solve Equation C-9 for $\delta^*/\theta_w x = \delta^*/R$. A graphical solution obtained by reading off values of $\delta^*/\theta_w x$ from a graph of $\delta^*/\theta_w x$ vs. ζ determined from Equation C-9 is most convenient. A plot of Equation C-9 corresponding to the correlation formula (Equation C-2) is shown in Figure C-4.

$\delta^*/\theta_w x$ determines the effective test section area and consequently all the test section parameters. Thus

$$\frac{A_{eff}}{A_t} = \left(\frac{x\theta_w}{r_t}\right)^2 \left(1 - \frac{\delta^*}{\theta_w x}\right)^2 . \qquad \text{(C-10)}$$

Combining Equations C-5 and C-10 it follows that when $\frac{\gamma - 1}{2} M_e^2 >> 1$

$$M_e = \frac{\left[\left(\frac{x\theta_w}{r_t}\right)^2 \left(1 - \frac{\delta^*}{\theta_w x}\right)^2\right]^{\frac{\gamma - 1}{2}}}{f_1 \left(\frac{\gamma - 1}{\gamma + 1}\right)^{\frac{\gamma + 1}{4}}} \quad . \tag{C-11}$$

Knowing M_e, p_e and T_e can be calculated using Equations C-3 and C-4. The dimensionless free stream density can be computed from

$$\frac{\rho_e}{\rho_R} = \frac{p_e}{T_e}\left(\frac{T_R}{p_R}\right) \tag{C-12}$$

where ρ_R is the density at standard or reference conditions and where ρ/ρ_R is sometimes referred to as density in Amagat units.

The procedure described above combined with extensive cross plotting has been used to compute the results described in Section III of the main report. One source of error in the calculations above is that while Goin's tables, used to compute f_1 and f_2, are based on the most recent NBS calculations for real air,[6] the Blackwell Tables and the Feldman Mollier Diagram, used to calculate f_3 and ΔS are based on the older NBS data for argon free air.[71] In view of the large uncertainty introduced in using the empirical formulas for δ^*/x, the effects of the above inconsistency can be ignored.

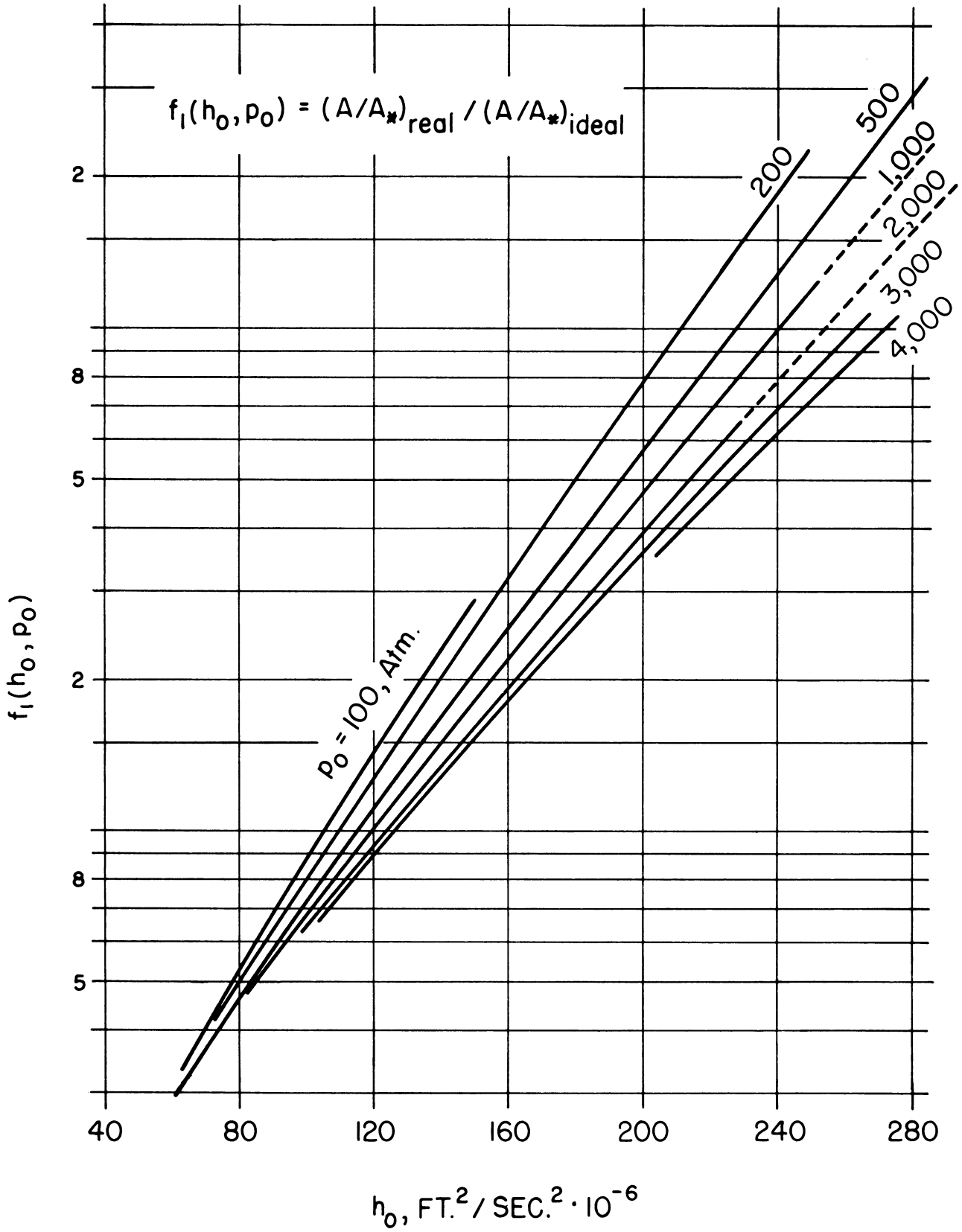

FIGURE C-1. AREA RATIO CORRECTION FACTOR $f_1(h_0, p_0)$.

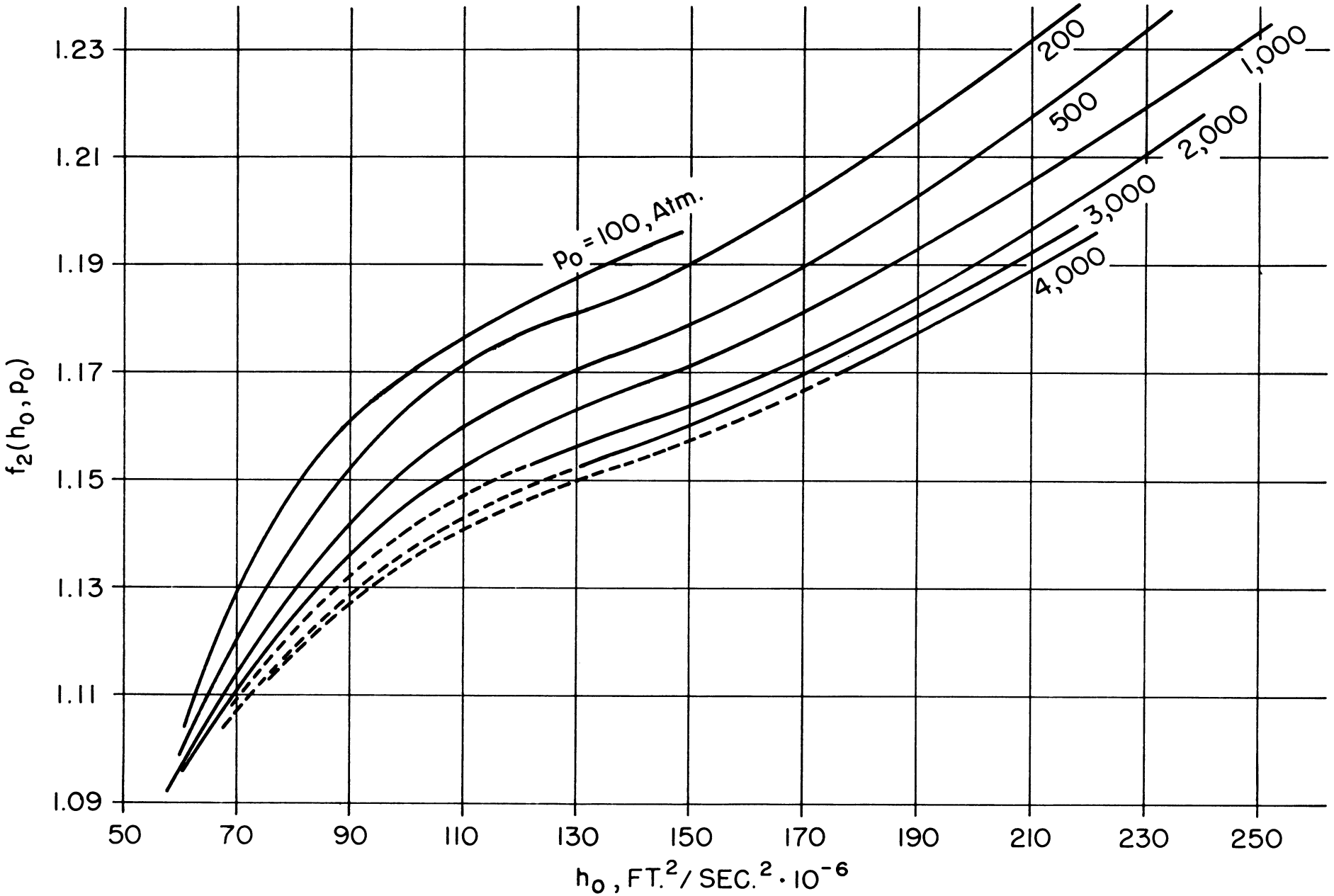

FIGURE C-2. MASS FLOW CORRECTION FACTOR $f_2(h_o, p_o)$.

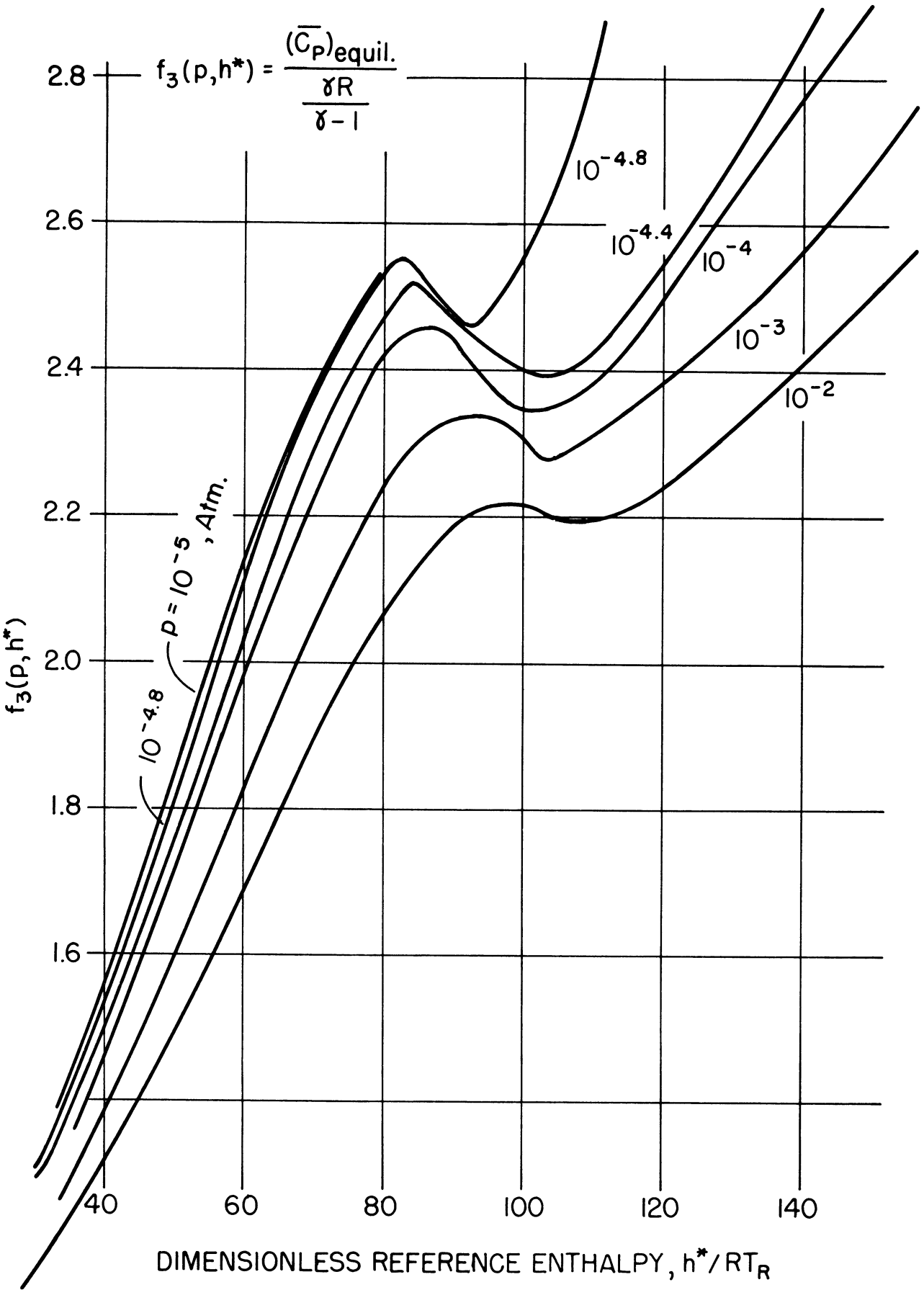

FIGURE C-3. RATIO OF AVERAGE TO IDEAL GAS SPECIFIC HEAT, $f_3(p,h^*)$.

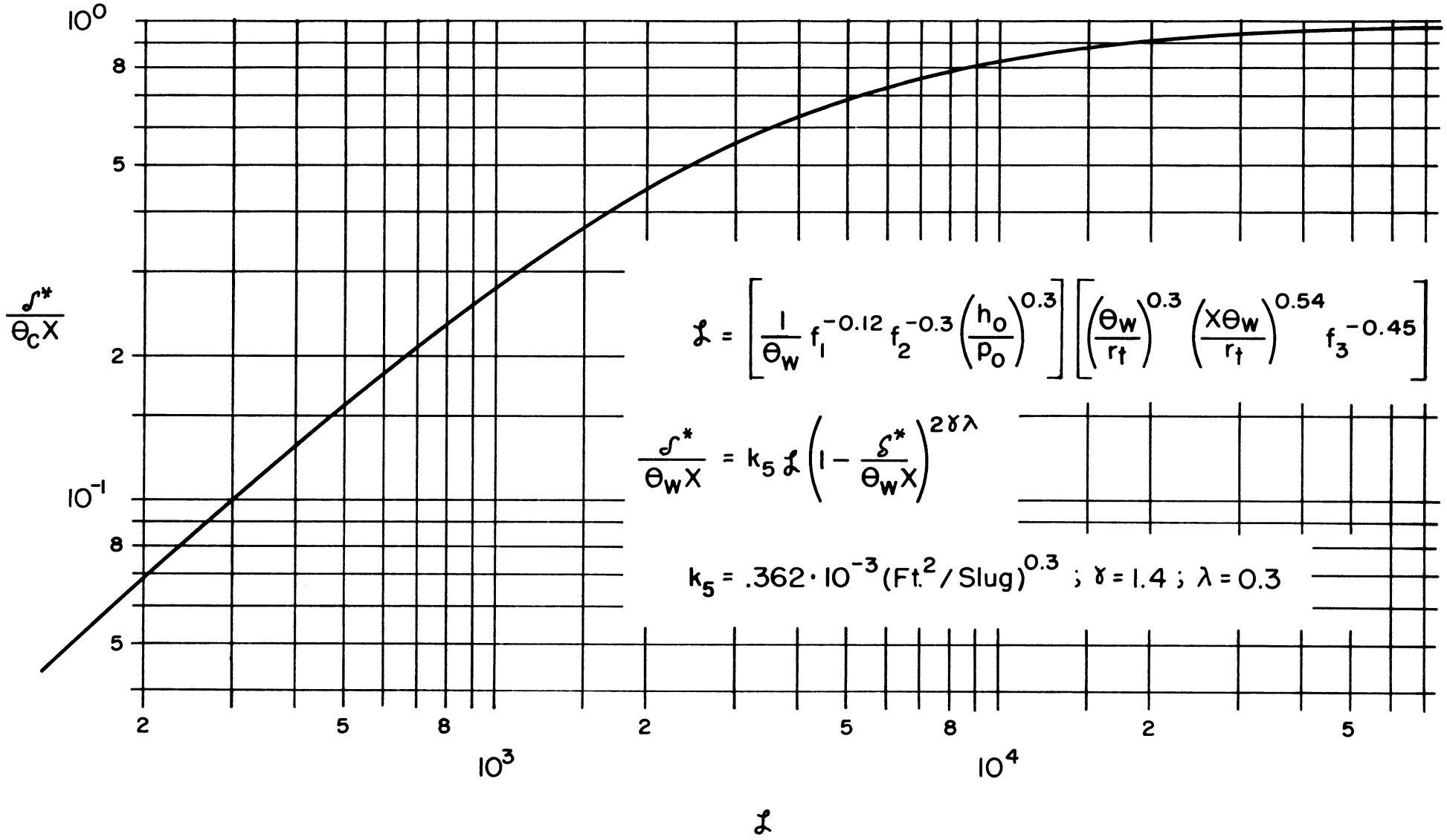

FIGURE C-4. VARIATION OF THE BOUNDARY LAYER THICKNESS WITH THE FUNCTION $\mathcal{L}$.